CHALMERS
UNIVERSITY OF TECHNOLOGY

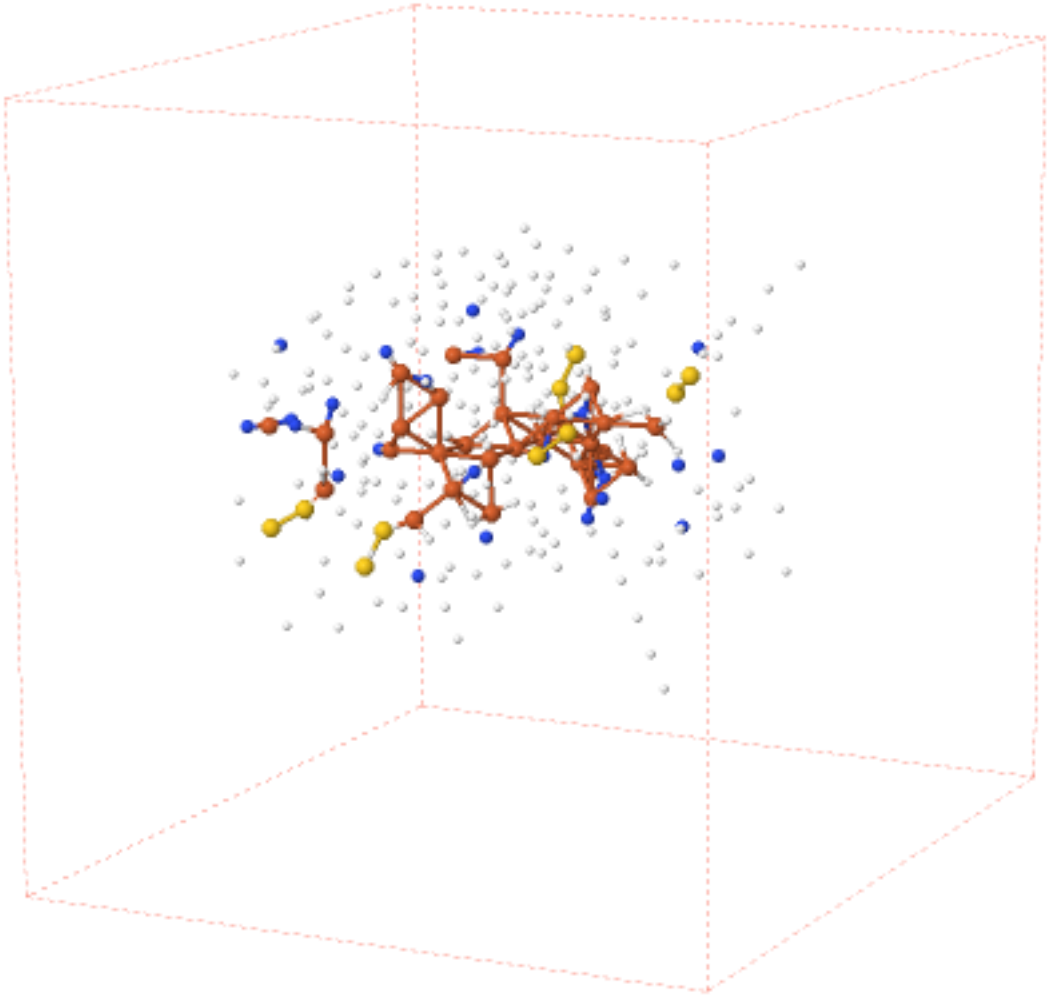

Optimization of parameters for ab initio molecular dynamics simulation of displacement cascades

Master's thesis in Nuclear Science and Technology

SRIRAM VENKATESAN

Department of Physics
CHALMERS UNIVERSITY OF TECHNOLOGY
Gothenburg, Sweden 2017

Master's thesis 2017:

Optimization of parameters for ab initio molecular dynamics simulation of displacement cascades

SRIRAM VENKATESAN

CHALMERS
UNIVERSITY OF TECHNOLOGY

Department of Physics
Division of Materials Microstructure
Chalmers University of Technology
Gothenburg, Sweden 2017

Optimization of parameters for ab initio molecular dynamics simulation of displacement cascades
SRIRAM VENKATESAN

Supervisor: Pär Olsson, Department of Physics, KTH Institute of Technology
Examiner: Mattias Thuvander, Department of Physics, Chalmers

Master's Thesis 2017:
Department of Physics
Division of Materials Microstructure
Chalmers University of Technology
SE-412 96 Gothenburg
Telephone +46 31 772 1000

Cover: Displacement cascade in Iron lattice done using DYMOKA, visualized using JMOL.

Typeset in LaTeX
Printed by Chalmers Repro Service
Gothenburg, Sweden 2017

Optimization of parameters for ab initio molecular dynamics simulation of displacement cascades
SRIRAM VENKATESAN
Department of Physics
Chalmers University of Technology

Abstract

Radiation can affect a material in many ways. Knowledge of this is vital in choosing the right material for application wherein the material is subjected to radiation. In nuclear fission reactors, materials inside the reactor vessel are exposed to radiations of all kinds. It is important to study their interaction with the materials because they affect the microstructure of the materials which in turn has a devastating effect on the macroscopic properties of the materials. With increase in computational power we have turned to Density Function Theory (DFT), semi-empirical Molecular Dynamics (MD) and other types of simulations to study the effect which can be verified with experimental techniques up to a certain extent. The aim of this thesis is to perform the first-ever simulations of displacement cascades using ab initio molecular dynamics (AIMD). To run these extremely costly simulations, it is paramount to first optimize various input parameters. Iron was chosen as it is widely used for structural components in reactors (as steel alloys). The optimizing simulations were done using MD simulations with semi-empirical Embedded atom method (EAM) potential in BCC iron with different input parameters including energy of the primary knock on atom (PKA), position of the PKA relative to damped boundary conditions, number of atoms, direction of the PKA and damping effects. It is essential to optimize because simulating large number of atoms significantly increases the time required for the simulation which also makes it more expensive to carry out the MD simulations. The other parameters are interrelated. For example, simulating with a high energy PKA in a small set of atoms distorts the results making them unacceptable. Damping coefficients also have to be optimized for the investigation as a strong damping will essentially quench the lattice. From the MD simulations, we could identify the ideal parameters. The influence of the number of atoms was found to be the most significant parameter which in turn decides the maximal PKA energy that can be simulated ab initio. The largest cell size that is possible to use with our current computer allocations is around 4000 atoms, limiting the maximal PKA energy to about 500 eV.

Keywords: molecular dynamics, CMD, ab initio, DFT, VASP, LAMMPS, Dymoka, displacement cascades, radiation damage, multi-scale modelling

Acknowledgements

அகர முதல எழுத்தெல்லாம் ஆதி
பகவன் முதற்றே உலகு

A, as its first of letters, every speech maintains; The "Primal Deity" is first through all the world's domains.

I would first like to extend my sincerest gratitude to my thesis supervisor Dr. Pär Olsson, Head of the Reactor Physics department at KTH Royal Institute of Technology. When I expressed my interest in his field of research, he took me under his wing and taught me so much in my field of thesis. I would like to thank him for the patience he showed in teaching and for sharing his invaluable time with me.

I would also like to thank Dr. Mattias Thuvander, Associate Professor, Department of Physics at Chalmers University of Technology for giving me the initial spark to take up nuclear materials and pointing me in the right direction.

To one of my biggest inspiration, to my former manager Mr. KNM, retd. Sr. GM at TVS Motor Company, I would like to express my gratitude for motivating me towards higher studies and giving me the courage to quit my job and grab my chance. Only by letting go of something we can grab another bigger thing. Thank you sir.

Thanks to my friends Navin, Sharme, Siva, Nithi, and Vidya for supporting me and for being there for me during the tough times, from thousands of miles away in India. Many thanks to my classmates, Niklas, Johan and Jessica for making my time in Sweden enjoyable and fruitful. I will forever cherish those memories.

A lot of people have helped me in becoming whom I am today, and none more than my parents, aunt, uncle and family. They supported when I chose pursue my dream; to them I owe my life. To my sister Sriranjani, I owe special thanks for being the sweetest sister one can ask for.

I would also like to acknowledge the Avancez scholarship provided by the Chalmers Foundation without which this wouldn't have been a possibility.

Sriram Venkatesan, Gothenburg, October 2017

Abbreviations and nomenclature

List of abbreviations

AIMD	Ab-initio molecular dynamics
APW	Augmented plane wave
BCC	Body-centered cubic
BWR	Boiling water reactor
CMD	Classical Molecular Dynamics
DFT	Density Functional theory
EAM	Embedded atom method
FCC	Face-centered cubic
GB	Grain boundaries
HEG	Homogeneous gas theory
IRSCC	Irradiation stress corrosion cracking
keV	Kilo electron volts
KMC	Kinetic Monte Carlo
LDA	Local density approximation
LWR	Light water reactors
MeV	Million electron volts
PAW	Projector augmented wave
PBC	Periodic boundary condition
PKA	Primary knock-on atom
RIS	Radiation induced segregation
RPV	Reactor pressure vessel
SIA	Self-interstitial
SS	Stainless steel
TDE	Threshold displacement energy
UTS	Ultimate tensile strength
VASP	Vienna Ab-initio Simulation Package
YS	Yield strength

Element symbols

Bi	Bismuth
C	Carbon
Cr	Chromium
Cu	Copper
Fe	Iron
Mn	Manganese
Mo	Molybdenum
N	Nitrogen
Ni	Nickel
O	Oxygen
P	Phosphorous
Si	Silicon
Sr	Strontium
U	Uranium
Xe	Xenon

Physical quantities

E_d	Displacement energy
R_d	Displacement rate
E_c	Electronic cut-off energy
T	Energy of the PKA
ϕ	Neutron flux
σ	Nuclear cross section

Contents

Abstract v
Acknowledgements vii
Nomenclature ix
List of Figures xiii
List of Tables xv

1 Introduction **1**
1.1 Background 1
1.2 Nuclear Fission 2
1.2.1 Nuclear reactor 3
1.2.2 Reactor materials 3
1.3 Nuclear fusion 4
1.3.1 Fusion reaction 5
1.3.2 Fusion materials 6
1.4 Motivation 6
1.5 Aim 6

2 Radiation damage in materials **9**
2.1 Introduction 9
2.2 Neutron irradiation 10
2.3 Displacement cascades 11
2.4 Displacement theory 12
2.4.1 Kinchin and Pease model for displacement 12
2.4.2 Modifications to the K-P model 13
2.5 Microscopic effects and macroscopic evolution 15
2.5.1 Diffusion and concentration of defects 15
2.5.2 Radiation induced segregation 17
2.5.3 Embrittlement and hardening due to irradiation 18
2.5.4 Irradiation creep and swelling 19

3 Modelling techniques **21**
3.1 Ab-initio Molecular Dynamics 21
3.1.1 Schrodinger equation 21
3.1.2 Born-Oppenheimer approximation 22
3.1.3 Variational principle 22
3.1.4 Hohenberg-Kohn-Sham formulation 23
3.2 Approximation methods in DFT 24

3.2.1 Local Density Approximation 24
3.2.2 Pseudopotential approximation 25
3.2.3 Augmented plane wave method 26
3.2.4 Projector augmented wave method 26
3.3 Classical molecular dynamics 27
3.3.1 Embedded atom method potential 28

4 Cascade modelling **31**
4.1 MD simulation condition and parameters 31
4.1.1 Size of super-cell and energy of PKA 31
4.1.2 Direction & position of PKA and damping effects 31
4.1.3 Initial condition for simulation 32
4.2 Ab-initio simulation 32

5 Results and discussions **33**
5.1 Influence of cell size and energy of PKA 33
5.2 Damping effects on the boundary 36
5.3 Effect of position of the PKA 38

6 Conclusions **41**
6.1 Future Work 42

Bibiliography **43**

List of Figures

1.1 Neutron cycle in a reactor 2
1.2 Schematic representation of a BWR 3
1.3 Materials used in a BWR 4
1.4 Cross section for fusion reactions 5

2.1 Crystal lattices 9
2.2 MD simulation in BCC iron lattice of approx. 5500 atoms at 50K with a PKA of $500eV$ 11
2.3 Displaced atoms as a function of PKA energy T 13
2.4 Schematic representation of channeling of an atom in the crystal lattice 15
2.5 Vacancies (a) and interstitial (b) fractions and their respective cluster size for different PKA atoms 16
2.6 Radiation induced segregation of Cr, Ni, Si and P at the grain boundary 17
2.7 Effect of damage mechanisms on irradiation embrittlement of RPV steel 19
2.8 Effect of hardening on a) FCC b) BCC metals 19
2.9 Isotropic swelling in 20% CW 316 irradiated to 80 dpa at 510°C in a fast reactor, (linear dimension +10%) 20

3.1 Schematic representation of the potentials and their wavefunctions . . 25

5.1 Number of vacancies vs cell size for direction $\langle 135 \rangle$ 34
5.2 Standard error in simulations 35
5.3 Comparison of defect formation in different directions (300eV) 36
5.4 Effect of damping on large and small cells (300ev in $\langle 135 \rangle$) 37
5.5 Different positions for the PKA 38
5.6 Effect of PKA positions in a large cell (300ev in $\langle 135 \rangle$ for 5460 atoms) 39
5.7 Effect of PKA positions in a large cell (300ev in $\langle 135 \rangle$ for 1980 atoms) 39
5.8 Effect of PKA positions in a large cell (500ev in $\langle 135 \rangle$ for 5460 atoms) 40

List of Tables

1.1 Fusion reactions 5

2.1 Defect reaction and annihilation 10
2.2 Types of neutron matter interaction 10
2.3 Time-scale of events 11

1

Introduction

The energy demand for the world is ever increasing. We have found various sources to quench our energy thirst with coal being the most popular in olden days. As our technologies developed we found more attractive energy sources including hydro, nuclear, wind and solar. In today's world, not only the energy demand is a concern but also the side effects that come along with it. Emission of greenhouse gases and the global warming it causes is the primary problem. The solution is for us to move towards cleaner energy sources that can match coal in terms of cost and capacity to match the demand. Nuclear energy for one can replace coal. It is an emission free energy source and can supply the huge demand that we have now. With nuclear energy in production we also have the radioactive wastes it generates. We must take up responsibility for the proper disposal of the nuclear waste. Countries like Sweden and Finland are far ahead of the world in handling the radioactive waste. Many other countries also have plans for proper disposal of the waste. For the time being, nuclear energy is the viable source for large scale emission free energy. Fusion energy is another attractive source of energy. Extensive research has been going on for the past decade with projects like ITER, JET, Wendelstein 7-X in Europe, EAST in China. Fusion energy source has many advantages like reduced high level radioactive waste and an essentially inexhaustible fuel source. However, we are still many decades from a commercially operating fusion reactor.

1.1 Background

Utilizing the nuclear energy requires the use of special materials that can withstand the conditions inside a nuclear reactor. It requires the use of materials that can sustain the damage caused by radiation among other requirements. Developing materials for these applications requires knowledge about the kind of the damage that occurs and understanding about the many mechanisms involved. As we know there are different kinds of radiation and they can cause different kinds of damages which we will discuss later. In this work, we concentrate on the damage created in iron by neutron irradiation by performing molecular dynamics (MD) and density functional theory (DFT) simulations.

1.2 Nuclear Fission

The principle behind the working of a nuclear reactor is the fission of atoms. When certain heavy atoms like uranium or plutonium are struck by neutrons, they can split into two lighter atoms. The difference in mass between the fission products and the reactants is liberated as energy. One fission event in case of ^{235}U shown in equation 1.1 gives about 200 MeV of energy.

$$^{235}_{92}\mathrm{U} + ^{1}_{0}\mathrm{n} \rightarrow ^{140}_{54}\mathrm{Xe} + ^{94}_{38}\mathrm{Sr} + 2^{1}_{0}\mathrm{n} + 200MeV \tag{1.1}$$

The fission of $^{235}_{92}$U gives two fission fragments as shown. But this is not the only way a fission can happen and it can happen in more than 30 different ways. The fission energy is liberated in the form of radiation and mostly is constituted in the kinetic energy of the fission fragments. This kinetic energy is converted to heat. On average 2.43 neutrons are emitted from a thermal fission in ^{235}U (see equation 1.1). These neutrons contain about 5 MeV of the fission energy. The neutrons from the fission reaction cause further fission events and this is a self-sustaining and self-propagating chain reaction. A nuclear reactor is a place where we sustain a chain reaction in a controlled and safe way. The neutrons emitted from fission reactions are fast neutrons and have energy of about 2 MeV. Most of our reactors use thermal neutrons for the fission process. So, we slow down the neutrons by numerous collisions. Moderators are used for slowing down fast neutrons to thermal neutrons.

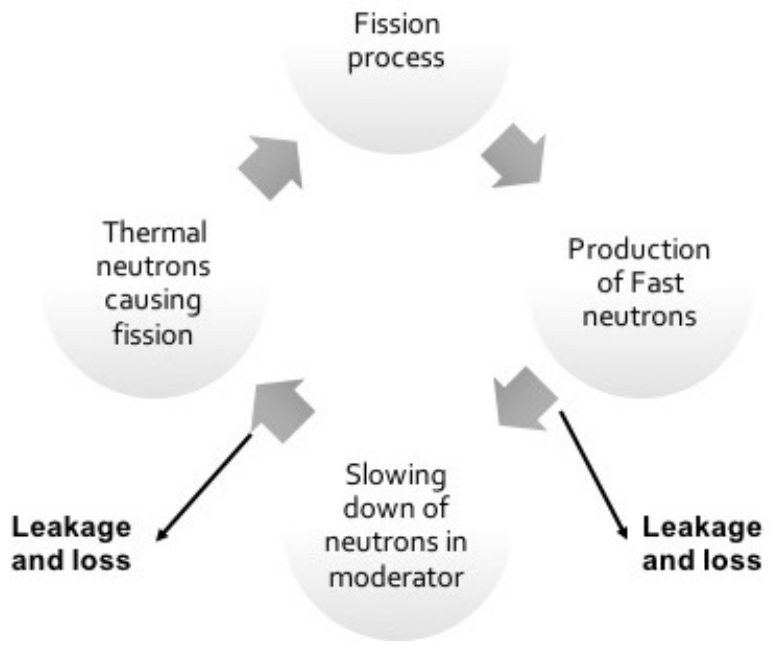

Figure 1.1: Neutron cycle in a reactor

During this neutron life cycle shown in the figure 1.1, some of the fast escape and are not slowed down and similarly some of the thermal neutrons do no cause fission

and are scattered or lost. These neutrons are absorbed by the components of the reactor pressure vessel, thereby irradiating them.

1.2.1 Nuclear reactor

A nuclear power plant uses the heat from the fission reactions to produce electricity. The image 1.2 shows the schematics of a simple boiling water nuclear power plant (BWR).

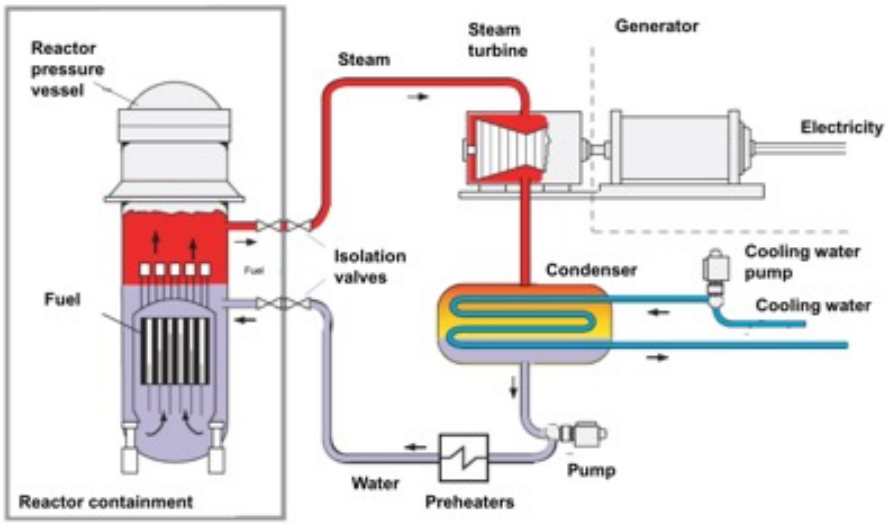

Figure 1.2: Schematic representation of a BWR [1]

The power plant comprises a reactor pressure vessel surrounded by the reactor containment. The fuel is present in the core of the reactor along with the control rods. The core is where the fission reaction occurs. The fuel is encased in fuel rods and multiple fuel rods are bundled together in fuel assemblies. A core may contain hundreds of fuel assemblies. The structural materials for the core that hold the fuel assemblies and the reactor pressure vessel are the primary components for safety. All kinds of radiation and fuel are contained inside it. To ensure safe operation of the reactor, the structural materials should be able to function at high temperature and exposure to radiation. The integrity of the structure should not be compromised at any state. Also, they must be able to function for a long time with less maintenance as shutting down for maintenance can prove costly.

1.2.2 Reactor materials

The materials used inside a reactor are tailor made to withstand the hostile conditions not present elsewhere. The working temperature can exceed 300°C in current generation reactors and significantly higher in future generation reactors. Combining this with high stress, corrosive environment and radiation exposure is something

that regular materials are challenged to withstand. From the figure 1.3, we can see that we have a variety of steel alloys present in the reactor.

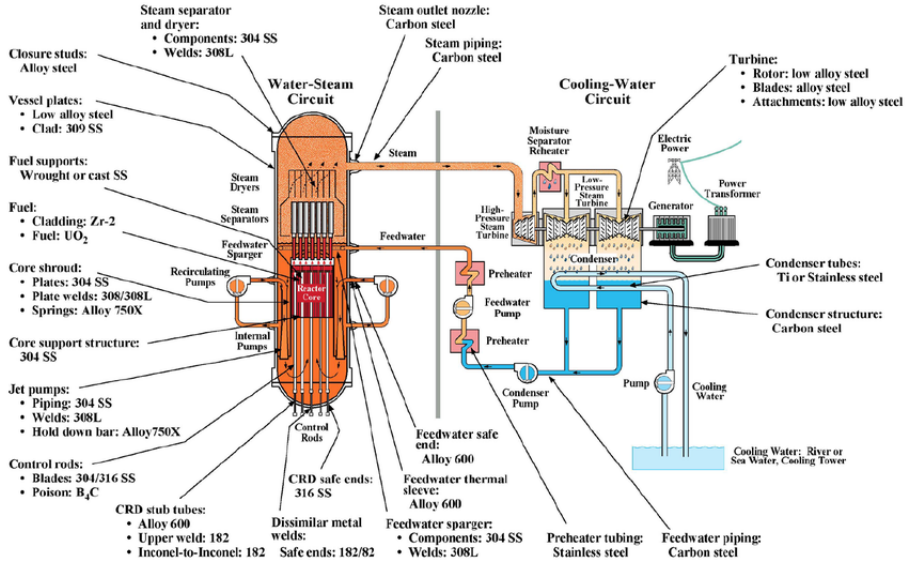

Figure 1.3: Materials used in a BWR [2]

We have Molybdenum alloyed steels for high corrosion resistance in control rods, common austenitic stainless steel like the 304 series for the pipes, low carbon iron alloys for the internal support structures, low alloy steel for the pressure vessel with high temperature resistant steel alloys as cladding. These steel alloys have extensive applications in the world. Martensitic steels are also used for their reduced swelling under irradiation.

1.3 Nuclear fusion

Fusion energy is an energy source for the future. The energy obtained from nuclear fission is by splitting a heavy atom. In fusion two light nuclei are fused and the difference in mass is emitted as energy. Fusion energy is potentially a much cleaner source for generating electricity. Like the conventional nuclear power plants fusion energy is also an emission free source. Fission energy generates tonnes of high level radioactive wastes which has to be handled with caution and be disposed in dedicated facilities. This is one of the major problems, the conventional nuclear power energy is facing. On the other hand, fusion does not generate significant levels of high level radioactive waste. The catch is that it is extremely difficult to sustain a fusion reaction. For fusion reactions to occur the Lawson criterion [3] has to be achieved. It provides the minimum plasma density n_e and confinement time τ_E that has to be met. This is extended in to the triple product. A fusion reaction can be self-sustaining if the product of density, temperature and confinement time is greater than a certain value. The ignition criterion is given by below expression.

$$\hat{n}\hat{T}\tau_E > 5.10^{21} m^{-3} keV s \tag{1.2}$$

1.3.1 Fusion reaction

Fusion energy uses the isotopes of Hydrogen, Deuterium (D) and Tritium (T) as fuel to produce Helium (He) and energy. There are different reactions that can take place. Below are listed some of the possible fusion reactions.

Table 1.1: Fusion reactions

Reaction	Equation	Energy (MeV)
$D-T$	$D+T \rightarrow^4 He+n$	17.6
$D-D$	$D+D \rightarrow^3 He+n$ (50%)	3.27
$D-D$	$D+D \rightarrow T+p$ (50%)	4.03
$p-^{11}B$	$p+^{11}B \rightarrow 3^4He$	8.7

There are other fusion reactions like p-p, D$-^3$He, H-D and T-T etc. But the reaction cross section is quite low for other reactions and consequently the temperature required is higher. For fusion to take place the fuel is heated to the order of a hundred kilo electron volts (keV). The cross section for different fusion reactions as a function of temperature is given in the figure 1.4. Note that the temperature is given in energy unit keV instead of Kelvin. The unit keV corresponds to a temperature of about 100 million Kelvin through the relation $E = k_B T$ where k_B is the Boltzmann constant with a value of $1.38.10^{-23}$ J/K and $1eV = 1.6.10^{-19}$ J [4].

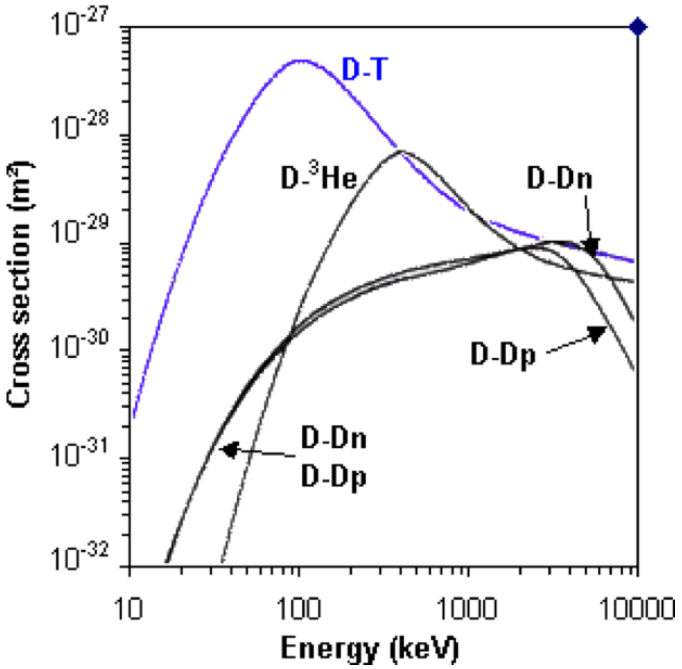

Figure 1.4: Cross section for fusion reactions [5]

From the figure 1.4, we can see that the D-T reaction is favourable because of its high cross section for low energies. But still we require about 100 keV to sustain the

D-T reaction. From the table 1.1 we can see that the energy output is also quite high for the D-T reaction. However, there is an emission of high energy neutron (14.1 MeV) which is very high compared to fission reactions. The walls of the fusion reactor must be able to shield the external components from this flux of high energy neutrons. This is where radiation damage becomes critical for fusion reactors. The ideal reaction for a fusion reactor would be the p$-^{11}$B as it has no emission of neutrons and only α emission. Also it is possible to convert that energy directly into electricity by slowing down the ions in an electric field or by using a magnetic field to spiral the ions and capturing the synchrotron radiation [4, 6, 7].

1.3.2 Fusion materials

With a flux of high energy neutrons (>10 MeV) and higher working temperature than a nuclear fission reactor, fusion reactors require special materials. Fusion reactor walls require materials capable of sustaining very high temperatures as the heat load on the plasma facing wall can exceed 4 MW/m^2 with the divertor being able to take up to 10 - 20 MW/m^2 [8, 9]. Many different kinds of materials are needed for a fusion reactor, including steels, refractory materials, ceramics, superconductors, etc. A new class of materials like equiatomic single phase alloys with high temperature stability and resistance to radiation damage are being studied for fusion [10]. For fusion tungsten and its alloys remain as the popular material for fusion applications because of its high temperature stability, high crystallization temperature, thermal conductivity and neutron radiation resistance [11–14].

1.4 Motivation

The necessity to study the radiation effects arose from the fact that it has a devastating effect on the materials. We shall discuss the neutron irradiation effects on steel alloys primarily as it is used in reactor pressure vessels. Neutrons can knock out atoms from their lattice sites and can cause displacements thus creating defects. On long term exposure, these defects grow to affect the macroscopic properties of the materials including brittleness, irradiation hardening, swelling, irradiation stress corrosion cracking (IRSCC) due to radiation induced segregation (RIS) etc. Numerous studies have been conducted to understand the effect of neutron radiation on physical properties. The macroscopic effects of irradiation are discussed in section 2.5.

1.5 Aim

The aim of this work is to optimize the various input parameter for simulating displacement cascades in iron. First we need to understand the input parameters that are required to simulate a displacement cascade. The parameters are then chosen

and several simulations are run with different cases and analyzing the end state of the lattice by studying the number of vacancies and interstitials formed. The position of the defects, their migration in the lattice and the cluster formations have to be analyzed. The simulations are run using classical molecular dynamics (CMD) with embedded-atom method (EAM) interatomic potentials. The code used in this work is Dymoka. In this work, we study the effects of neutron irradiation in a single atom lattice. Upon analyzing the results presented in chapter 5, the input parameters like the cell size and energy of the primary knock on atom (PKA) are finalized. Using these parameters, similar simulations are then run using ab initio molecular dynamics (AIMD) in the Born-Oppenheimer approximation, using the Vienna Ab-initio Simulation Package (VASP). Running AIMD simulations require huge computational resources and it is important to first have the optimal parameters.

2

Radiation damage in materials

This chapter is written to provide an overview on how irradiation damage occurs and the macroscopic effects on the material properties.

2.1 Introduction

The atoms in a metal or alloy are arranged in a periodic order. Those with this kind of ordered structure are called crystalline solids while others are called amorphous or non-crystalline. The crystal structure is a repetition of a unit cell. Some examples of the crystal lattices are shown in the figure 2.1.

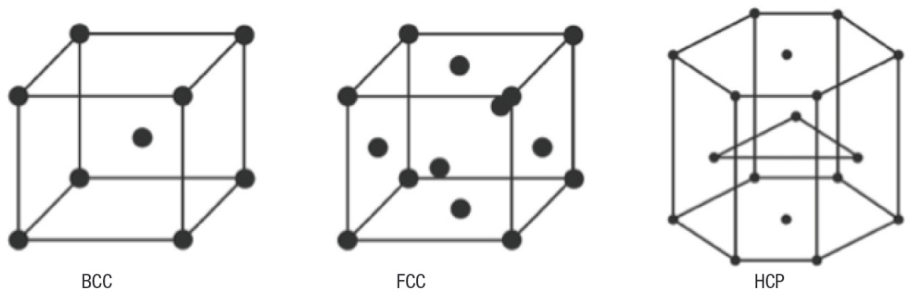

Figure 2.1: Crystal lattices

As seen in the figure 2.1, in body-centered cubic (BCC) crystal we have one atom in the center of the cube surrounded by one atom in each corner of the cube. In face-centered cubic (FCC), there is one atom in the center of each face of the cube and one in each corner. These are the common structures found in metals. This determines some of the properties of the metals. It can define how a defect behaves and propagates in the lattice etc.

The site occupied by the atoms at equilibrium are called lattice sites. Upon irradiation by neutrons, some of the neutrons interact with the atom by striking it and displacing it from its original site in the lattice. This is called the damage event. The striking neutron transfers some of its energy to the atom and the atom is subsequently displaced. This gives rise to point defects like interstitials and vacancies.

An atom occupying the position in between lattice points are called interstitials. In case of two atoms sharing the same lattice site, they are called split-interstitial or dumbbell pairs. If a lattice site is unoccupied, it is called a vacancy. Accumulation of these defects results in changes to the macroscopic properties of the material. The below table 2.1 shows how modes of defect behavior in a crystal. The disappearance or annihilation is when a vacancy and an interstitial recombine or when they reach the grain boundary (GB). The defects migrations can also cause accumulation of defects at dislocations or can result in the change in the size of a void.

Table 2.1: Defect reaction and annihilation [15]

Reaction	Result
Vacancy + SIA	Recombination
Vacancy + Vacancy	Di-Vacancy
Vacancy/SIA + GB	Disappearance
Vacancy/SIA + Dislocation	Disappearance / accumulation
Vacancy/SIA + Void	Disappearance / change in size of the void
Vacancy/SIA + Incoherent precipitate	Disappearance
Vacancy/SIA + Solute/Coherent precipitate	Segregation
SIA + SIA	Di-SIA

2.2 Neutron irradiation

Amongst radiations, the damage caused by neutrons will be discussed in this section. Since the neutrons do not contain any charge, it can interact with the nuclei as it does not have to overcome the Coulomb barrier and can pass very close to the nucleus unperturbed by the electrons. When a material is exposed to neutron radiation, the neutrons interact with the atoms in the lattice and can result in different reactions. The table 2.2 shows the various modes of neutron-matter interaction.

Table 2.2: Types of neutron matter interaction [16]

Reaction	Event
(n,n)	Neutron scattering
(n,n'), $(n,2n')$	Neutron absorption and emission
(n,p), (n,α)	Emission of charged particle
(n,γ)	Gamma emission
(n,f)	Nuclear fission

During elastic collisions, the neutron hits the atoms and is scattered. Some energy of the neutron can be transferred to the atom and the total energy of the system is conserved. This is more prevalent in neutron energies less than 1 MeV. During in-elastic scattering, reaction like charged particle emission and neutron absorption occur and there is a loss of energy in the system and this is dominant at energies

greater than 1 MeV. The time-scale for the events are quite small and occur almost instantaneously. The time-scale of the (n,n) event from table 2.2 is shown in the table 2.2

Table 2.3: Time-scale of events [1]

Times(s)	Event
10^{-18}	Neutron interaction and energy transfer to the PKA
10^{-13}	Atoms displaced by the PKA
10^{-11}	Dissipation of energy, spontaneous recombination and clustering formation
10^{-8}	Migration of defects

2.3 Displacement cascades

The collision cascade or the displacement cascade is the short spike in the number of displaced atoms. After this, the vacancies and interstitials that are close start recombining or diffusing in the lattice. The evolution of the cascade is exemplified in figure 2.2.

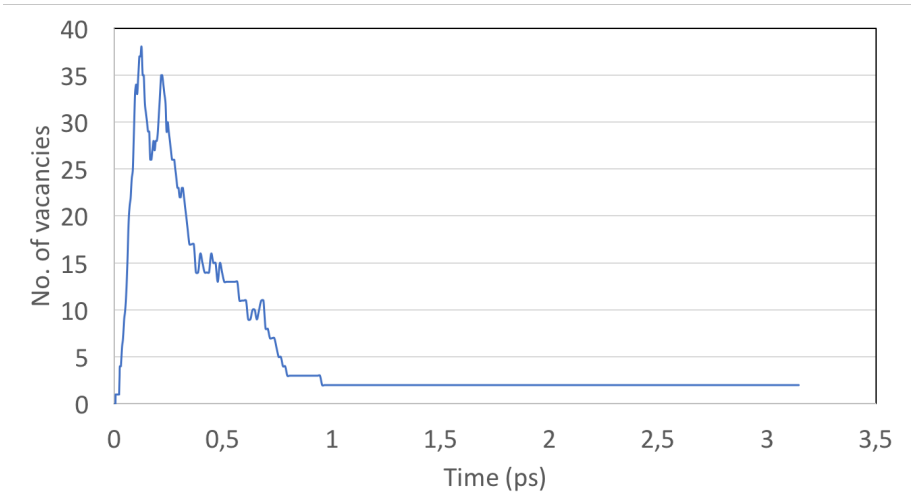

Figure 2.2: MD simulation in BCC iron lattice of approx. 5500 atoms at 50K with a PKA of $500eV$

From table 2.3 and figure 2.2, we know that the displacement cascade occurs over the first picosecond. The evolution of the cascade can be divided into 4 stages. First is the creation of the PKA and successive collisions until the energy of the successively displaced atoms fall below the TDE and can displace no more atoms. The second stage is where we witness a thermal spike. This is because all the collisional energy contained in the displaced atoms is deposited in the neighbouring atoms. At this point some parts of the lattice may contain high enough energy that they resemble

molten metal. The thermal spike requires about $0.1ps$. The third stage is the quenching stage where the energy is transferred to the lattice and is diffused through the surrounding atoms. It take about $10ps$ to get to thermodynamic equilibrium. In the presented case (figure 2.2) the amount of energy deposited in the lattice by the $500eV$ neutron is diffused throughout the 5500 atoms in the lattice. This may take a few ps. During this stage, the defects (vacancies and interstitials) that have not disappeared start to stabilize. The final stage is the annealing stage. Here we witness migration of defects away from the cascade and cluster formation or annihilation when they reach sinks. The timescale for this can extend up to months or years depending on the temperature.

2.4 Displacement theory

To understand the effect of irradiation we need to quantify it. The damage rate is the number of atoms displaced per unit time and volume depends on the energy of the incident neutron and the displacement cross section of the material.

$$R_d = N \int_{\check{E}}^{\hat{E}} \phi(E_i, T)\sigma_D(E_i)dE_i \tag{2.1}$$

and,

$$\sigma_D(E_i) = \int_{\check{T}}^{\hat{T}} \sigma_D(E_i, T)v(T)dT \tag{2.2}$$

Here R_d is the displacement rate, N is the lattice atom density. ϕ is the energy-dependent neutron flux and σ_D is the energy-dependent cross section. σ_D is dependent on the probability for the neutron of energy E_i to transfer an energy T to the atom. $v(T)$ is the number of atoms displaced by the collision which is dependent on the threshold displacement energy E_d of the material. E_d is the minimum energy required to displace the atom from its lattice site. Now the probability of an atom being displaced is 1 if the transferred energy T is greater than E_d. For $T<E_d$ it is 0. Also for a crystal the E_d can vary depending on factors like the crystal structure and the direction of the PKA. Hence we have two values $E_{d_{min}}$ and $E_{d_{max}}$. For values of T ranging between $E_{d_{min}}$ and $E_{d_{max}}$ the displacement probability is a smoothly varying function between 0 and 1.

2.4.1 Kinchin and Pease model for displacement

The number of displacements in the equation 2.2 has to be calculated. Kinchin and Pease developed a theory based on the following assumptions [17]

- The displacements are a series of events caused by independent two-body elastic collisions.
- The energy transfer is given by hard-sphere collision model.

- Electron stopping is given by E_c which is the cut-off energy. Collision happen only when $T < E_c$.
- There are no energy losses to the lattice. I.e for atom with energy T generating a new recoil with energy T_2 and emerging with T_1, $T = T_1 + T_2$.
- Displacement probability is 1 for $T > E_d$.
- The crystal structure is ignored. Therefore effects due to crystallinity like focusing and channeling are ignored.

The KP model provides the number of displaced atoms as

$$v(T) = \begin{cases} 0 & T < E_d \\ 1 & E_d < T < 2E_d \\ \dfrac{T}{2E_d} & 2E_d < E_c \\ \dfrac{E_c}{2E_d} & T \leq E_c \end{cases} \tag{2.3}$$

The number of displaced atoms as a function of the PKA energy is shown in fig 2.3

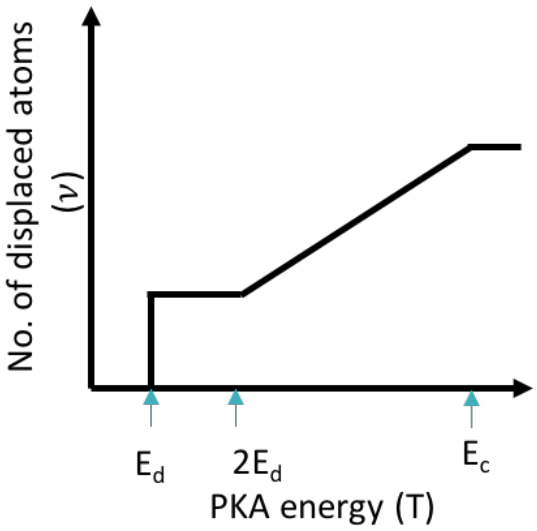

Figure 2.3: Displaced atoms as a function of PKA energy T

2.4.2 Modifications to the K-P model

Various modification have been done to the K-P including Snyder and Neufeld where the assumption 4 in the K-P model was changed. According to Snyder and Neufeld, both the atoms move off after collision irrespective of their energy and they added

another term to the energy loss relation as $T = T_1 + T_2 + E_d$. The effect of adding another term was compensated by the increase in the number of displaced atoms since the atoms are allowed to move even with low energies, so that the end model was similar to the K-P model [18].

$$v(T) = 0.56\left(1 + \frac{T}{2E_d}\right) \tag{2.4}$$

Lindhard et al. [19] proposed a model that includes the energy loss due to electronic excitation. The assumption is that even for energies $T > E_c$, there will be collisions and introduced an efficiency term in the equation 2.3 as such

$$v(T) = \xi(T)\left(\frac{T}{2E_d}\right) \tag{2.5}$$

Norgett, Robinson and Torrens proposed a method [20] with the efficiency term as a function of the PKA energy. ξ as such

$$v(T) = \frac{\kappa E_D}{2E_d} \tag{2.6}$$

where E_D is given by

$$E_D = \frac{T}{1 + k_N g(\varepsilon_N)} \tag{2.7}$$

Some of the problems with these models are that they work with hard-sphere approximation and the directional dependence of TDE. Effects due to crystallinity include channeling and focusing. Focusing is an effect that happens when the PKA is knocked in the direction along a high density atomic row like <100> or <111> in BCC. Consider an atom knocked in the direction θ with respect to the atomic row. If the angle is small enough, then the collision mimic a near head-on collision along the row of atoms and subsequent collisions will have a decreasing scattering angle. Channeling is the long-range movement of an atom along an open channel like passing through a long cylindrical tube by glancing off the walls of the tubes i.e. the row of atoms until its energy is lost (see figure 2.4). Channeling is a high energy phenomenon as the cross section for scattering is quite high for low energy ions. It occurs when the atom is knocked in a particular direction and there is a critical angle beyond which the atom cannot enter the channel. As the energy imparted to the atom increases, the critical angle decreases as the atom will knock on another atom instead of glancing off it [21].

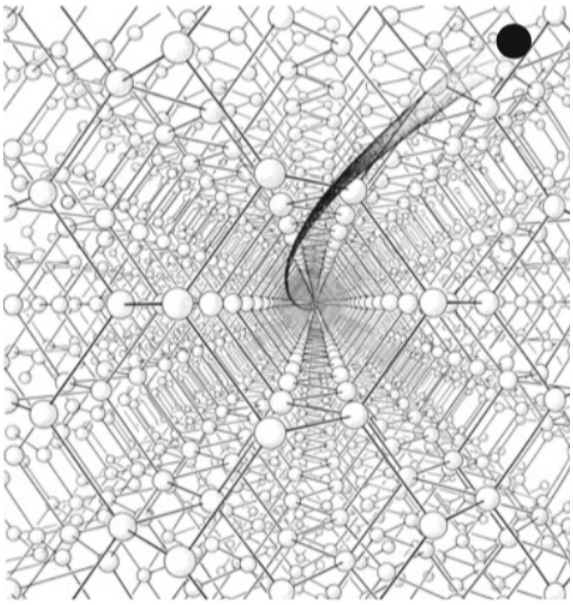

Figure 2.4: Schematic representation of channeling of an atom in the crystal lattice [21]

2.5 Microscopic effects and macroscopic evolution

Neutron irradiation in steel alloys and other metals and alloys result in deterioration of their mechanical properties and corrosion resistance. These are all caused by various effects of radiation like concentration of defects, segregation or depletion of alloying elements at grain boundaries, changes in the microstructure etc.

2.5.1 Diffusion and concentration of defects

Radiation can cause elevated concentration of point defects compared to thermal conditions. The formation and growth of defect clusters and migration of defects in displacement cascades have been well studied [22–25]. Studies have shown the presence of large interstitial clusters [26, 27]. A.F. Calder et al. conducted MD simulation of α-iron model with different PKA energies. Their studies showed the presence of large vacancies and interstitial clusters in a displacement cascade upon irradiation. It also showed that the probability of the formation of such clusters increased with the increasing mass of the PKA.

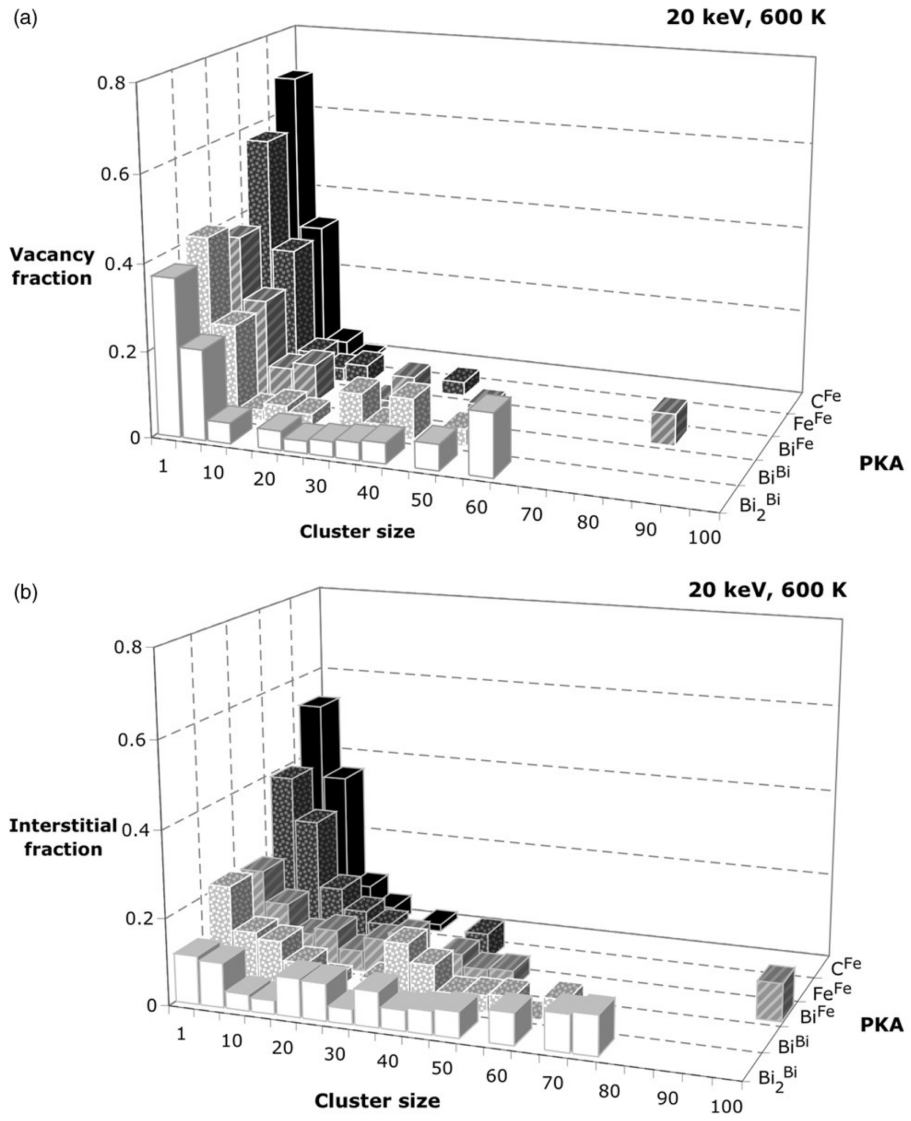

Figure 2.5: Vacancies (a) and interstitial (b) fractions and their respective cluster size for different PKA atoms [26]

A.F. Calder et al. conducted simulations with PKAs of C, Fe and Bi [26] and the results showed that the number of clusters and the size of the point defect clusters increases with increase in the mass of the PKA. However the total number of defects generated decreases with increase in mass. This however is pronounced more at lower energies. Also from the figure 2.5 we are able to see that at higher masses of PKA we have more number of larger clusters and reduced number of singles. It has also been shown that the fraction of vacancies and interstitials in clusters resulting from a cascade are different and depend on the temperature. The study by T.D.L. Rubia et al. on damage in FCC metals showed that cluster formation of defects is more pronounced in FCC than BCC metals. The presence of isolated clusters is more common in BCC metals than FCC [28].

The presence of solutes and other impurities also has some effect on the defects and

their mobility. The interaction of defects and solute atoms have been extensively researched. The presence of vacancies contributes to an increase in the clustering of the interstitial solute atoms like C, N and O [29] and substitutional solute atoms like Cr [30] in α-iron. The effect of solute atoms either substitutional or interstitial on the other hand have no effect on the number of defects or clusters resulting from a displacement cascade [30, 31] and Cr in Fe has no significant interaction with the vacancies [14]. There is also segregation of solute atoms with preference to a particular defect. A study by Ngayam-Happy et. al on MnNi and MnNiCu clusters in Fe alloys showed that segregation of MnNi precipitates is primarily on SIA clusters whereas Cu precipitation in Fe in vacancy driven [32,33]. The concentration of Cu precipitates discussed in the section 2.5.1 also lead to concentration of Mn precipitates around it [32].

2.5.2 Radiation induced segregation

Radiation induced segregation (RIS) is one of the most important problems faced in irradiated materials. This refers to the directionally biased movement of solutes or impurities present in metals. RIS results in enrichment or depletion of a particular solute at point defect sinks like grain boundaries (GB) or phase boundaries in alloys. There can also be saturation in the RIS effect. In stainless steel alloys there is a depletion of Cr and enrichment of Ni at grain boundaries [34, 35]. The figure 2.6 shows the RIS effect.

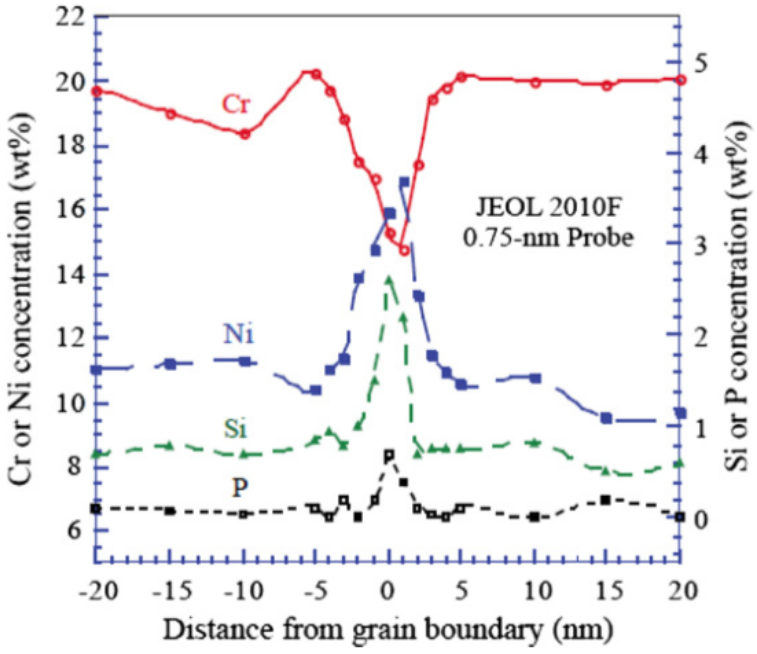

Figure 2.6: Radiation induced segregation of Cr, Ni, Si and P at the grain boundary [35]

It has also been shown that there is a preference for RIS depending on the type of GB.

Christopher M. Barr et al. [36] showed that the RIS was more pronounced in GB with incoherent twins in 316L austenitic SS. But having <110> Σ3 <111> coherent twin GB would not necessarily reduce the irradiation hardening effect because the GB would also act as a poor defect sink with a weak defect annihilation rate. Enrichment of P and depletion of Mo has been observed in 2.25Cr1Mo steel with P segregation not witnessed at lower temperatures in the study by S.H. Song et al [37]. It has been shown that there is a site competition between phosphorous and carbon at higher temperatures in Fe-C-P alloys. Presence of carbon or boron even in minor quantities can be effective in suppressing the enrichment of phosphorous at GB, with boron being more effective than carbon at temperatures higher than 500°C due to higher activation energy for diffusion in [38]. This is preferable as they improve the cohesive strength of the GB and reduces embrittlement [39].

2.5.3 Embrittlement and hardening due to irradiation

The above discussed effects like cluster formation, segregation, formation of voids and bubbles contribute to the deterioration of some mechanical properties. The resistance of the material to allow dislocation movement results in hardening. Segregation of phosphorous discussed in the section 2.5.2 results in embrittlement of the material. The increase in the number of defects and clustering of these defects also contribute to the increase in hardness. This increase in hardness can lead to embrittlement. Extensive research has been done on irradiation embrittlement on reactor pressure vessel (RPV) steels [40–42] as it is the most important safety component in the reactor and it cannot be replaced. It has shown that neutron induced hardening occurs on the high temperature corrosion resistant cladding which covers the inner wall of of the RPVs. Studies have shown that there are three main causes for embrittlement; presence of precipitates like Mn, Si, Cu, irradiation induced segregation of P at GB, and increase in number of defects in the bulk material.

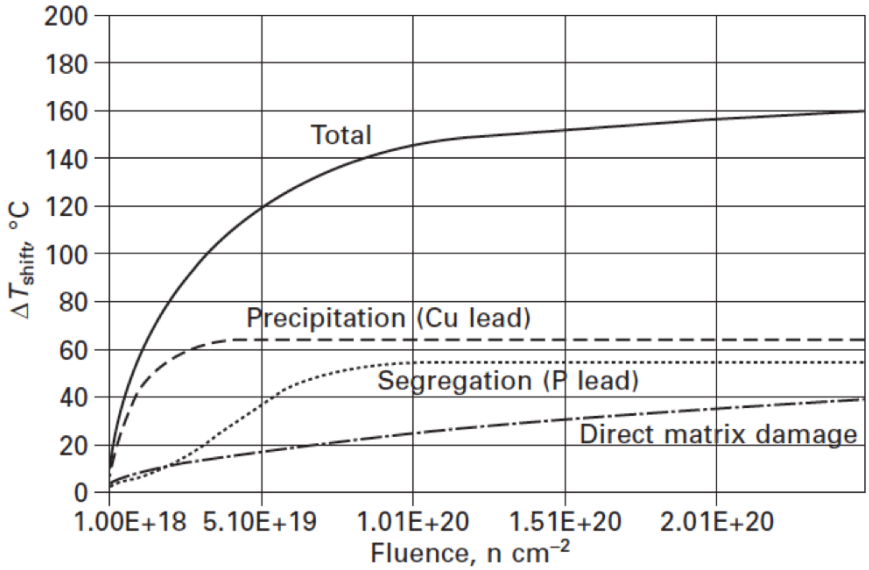

Figure 2.7: Effect of damage mechanisms on irradiation embrittlement of RPV steel [15]

From the figure 2.7, we can see that the Cu precipitation contributes the most to the embrittlement and the effect increases with increasing doses. Irradiation embrittlement and hardening lead to an increase in both yield strength (YS) and ultimate tensile strength (UTS) and reduction in the ductility (see figure 2.8). We can see that embrittlement is more pronounced in BCC metals and FCC metal show better ductility.

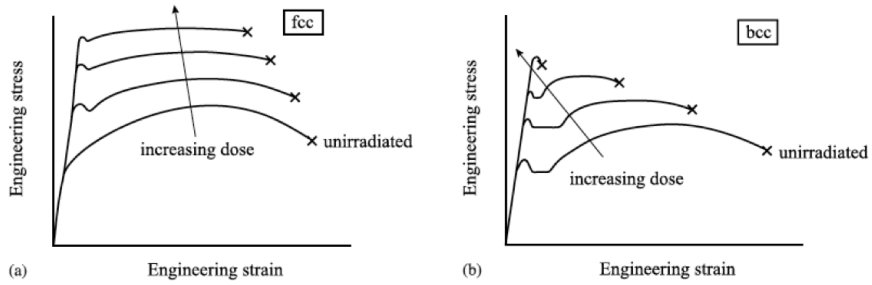

Figure 2.8: Effect of hardening on a) FCC b) BCC metals [43]

2.5.4 Irradiation creep and swelling

Creep in general is a time-dependent process which is accelerated due to irradiation. Creep is a failure of material under constant loading. In reactors, materials are subjected to high temperatures and high neutron flux for a long time. The production of defects due to irradiation leads to irradiation accelerated creep since it is mainly a diffusion-controlled phenomenon. It has been observed in SS and Zircaloys used in reactors. It was first observed in Fast breeder reactors as they had a higher flux and temperature compared to LWRs and this significantly increased the creep rate.

There are a couple of mechanisms for creep. In dislocation creep, the mobility of a dislocation is hindered by the presence of voids or loops, So it has to climb a slip plane and results in a pile up of blocked dislocations which results in an increased stress. Diffusional creep is due to the mobility of vacancies perpendicular to the stress direction when the materials is loaded and can accelerate the nucleation of dislocation loops. Materials undergo deformation during creep but the volume is conserved. Once the swelling start, creep is accelerated. [44]

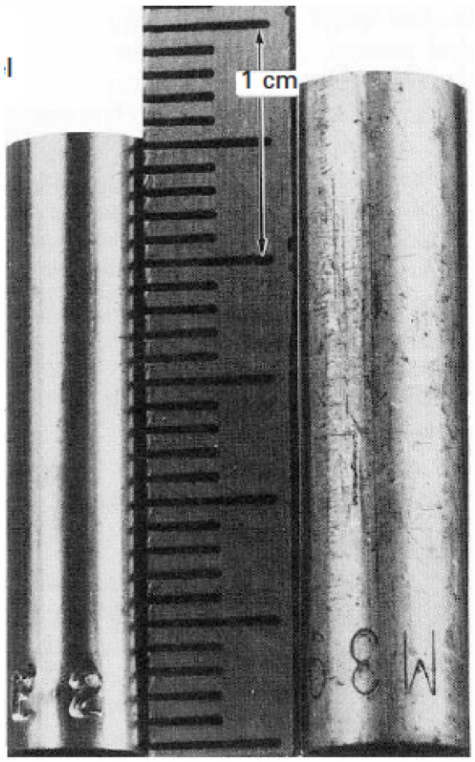

Figure 2.9: Isotropic swelling in 20% CW 316 irradiated to 80 dpa at 510°C in a fast reactor, (linear dimension +10%) [44]

The presence of an increased and unbalanced (by self-interstitials) number of vacancies is the driving force for swelling. Vacancies combine to form voids and voids nucleate to form bubbles. This leads to an increase in the dimensions of the material. Like RIS, swelling rate also saturates. Studies have shown that swelling rate saturation is worse in FCC compared to BCC. The formation of Helium bubbles from the production of α is also one of the contributors for swelling. Cold-worked steels and martensitic steel have markedly higher resistance to void swelling whereas annealed steels are more susceptible to swelling [45, 46]. Cold-working introduces more dislocations. Swelling has been found to be more severe in irradiated 304SS than in 316L.

3

Modelling techniques

The field of modelling the interaction between radiation and matter has grown by leaps and bounds in the past few years. The increase in processing power and development of more powerful supercomputers has helped us to perform more complex numerical simulations. Also with more accurate and reliable modelling methods we are able to bridge the gap between theory and experiments. Due to this, we have been able to study phenomenons that are not possible with experiments. In this chapter we will be looking at some methods that are employed to study materials on an atomic scale.

To perform simulations on an atomic scale we need to understand how atoms interact with each other and what are the forces acting on them and how the atoms respond. The laws of classical mechanics can be used to describe the forces acting on an atom. The basis is to model how the atoms position themselves with respect to others. If the position of one atom changes, then the other atoms interacting with that will change their positions relatively. It is a deterministic method where the movement of all the atoms are uniquely determined from their initial values by numerically solving the differential equations from Newtons second law of motion. This method is called molecular dynamics.

Replacing the classical mechanics with quantum mechanics, and by employing the Schrodinger equation, we can model the system with better accuracy. However, this is not possible without a few approximations. Even with the approximations, this method is computer intensive and can be employed for modelling up to a few picoseconds and a few thousand atoms. We will be seeing in detail about these methods in the upcoming chapters.

3.1 Ab-initio Molecular Dynamics

3.1.1 Schrodinger equation

Consider a system defined by its wavefunction Ψ. The wavefunction provides the probability distribution of all the nuclei and their associated electrons in the system.

The time-independent Schrodinger equation can be written as

$$\hat{H}\Psi_i(r_1, r_2, ...r_N, R_1, R_2, ...R_M) = E_i\Psi i(r_1, r_2, ...r_N, R_1, R_2, ...R_M) \tag{3.1}$$

The $\hat{H}$ is the Hamiltonian operator and r and R are the position vectors for the n electrons and M nuclei. The Hamiltonian operator is the sum of operators of kinetic energy and the potential energy which is the coulomb potential. Therefore the Hamiltonian can be written as

$$\hat{H} = T_e + T_n + V_{ee} + V_{nn} + V_{en} \tag{3.2}$$

Here T_e and T_n represent the kinetic energy of the electrons and nuclei, respectively, V_{ee} and V_{nn} represent the coulomb interaction potential between the electrons and nuclei respectively and V_{en} represents the coulomb interaction potential between the electrons and nuclei.

A direct numerical solution for the equation 3.1 is not possible. Hence we employ some approximations. They are based on the fact that electrons are much lighter and faster compared to the nuclei and hence split the equation in to two components, the electronic Schrodinger equation and the nuclei part. The nuclei part of the equation is further approximated with classical mechanics by using empirical potentials or effective potentials calculated from the quantum mechanical computations. The latter is called ab-initio molecular dynamics. It employs the fundamental interactions of the particles i.e we will be able to derive potentials without any approximations.

3.1.2 Born-Oppenheimer approximation

The Born-Oppenheimer approximation considers that the nucleus is significantly slower and much heavier than the electron and so the electron can adapt to any configuration of the nucleus instantaneously. Therefore they are always in the quantum mechanical ground state in comparison with the nucleus. Since the movement of the nuclei is negligible, the equations 3.1 and 3.2 can be written as

$$\hat{H}\Psi_i(r_1, r_2, ...r_N) = E_i\Psi i(r_1, r_2, ...r_N) \tag{3.3}$$

and

$$\hat{H} = T_e + V_{ee} + V_{en} \tag{3.4}$$

The solution to the electronic schrodinger equation provides how the electrons adjust to the position of the nuclei and it provides the effective potential to move the nuclei in the next time step.

3.1.3 Variational principle

The variational method helps us to find the true ground-state energy E_0. The principle states that the energy computed from a chosen trial wavefunction is the

upper bound to E_0. E_0 can be be found by minimizing the energy with respect to all wavefunctions of the associated electrons.

$$E_0[\Psi_0] = \min_{\Psi} E[\Psi] = \min_{\Psi} \langle \Psi | \hat{T} + \hat{V_{ee}} + \hat{V_{en}} | \Psi \rangle \tag{3.5}$$

and

$$E_0[\Psi] = \langle \Psi | \hat{H} | \Psi \rangle = \int \Psi^* \hat{H} \Psi(x) dx \tag{3.6}$$

3.1.4 Hohenberg-Kohn-Sham formulation

The Hohenberg-Kohn-Sham is one the approaches to DFT and is widely used. The first theorem of Hohenberg-Kohn states that the potential $\hat{V_{en}}$ is a unique functional of the electron density $\rho(r)$ which means that the total energy is also a functional of $\rho(r)$. This effectively means that all the properties of the system can be determined from $\rho(r)$. The second theorem states that the functional that delivers the ground state energy of the system gives the lowest energy only when the input density is the true ground state density. [47]

$$E_0[\rho_0] = \min_{\rho} E[\rho] = \min_{\rho} T[\rho] + E_{ee}[\rho] + E_{en}[\rho] \tag{3.7}$$

The Kohn-Sham approach builds on the Hohenberg-Kohn theorem stated above [48]. They introduce a non-interacting fictitious system with same density as the real system. The kinetic energy and electron density are given by

$$T_s[\rho] = \frac{1}{2} \sum_{i}^{N} \langle \Psi_i | \nabla_2 | \Psi_i \rangle \tag{3.8}$$

and

$$\rho(r) = \sum_{i}^{N} |\Psi_i(r)|^2 \tag{3.9}$$

The total energy of the system is given by

$$E[\rho] = T_s[\rho] + E_{xc}[\rho] + E_{en}[\rho] + E_H[\rho] \tag{3.10}$$

where we have the kinetic energy, $T_s[\rho]$, the nuclei-electron interaction functional $E_{en}[\rho]$,the Hartree energy $E_H[\rho]$ and the exchange-correlation energy $E_{xc}[\rho]$. This includes the difference in kinetic energy between the two systems, Coulomb interaction for the electrons of opposite spin, energy from the Pauli's exclusion principle and a self interaction term.

$$E_H[\rho] = \frac{1}{2} \int \int \frac{\rho(r_1)\rho(r_2}{r_{12}} dr_1 dr_2 \tag{3.11}$$

and

$$E_{en}[\rho] = \int V_{en} \rho(r) dr \tag{3.12}$$

Here the form of the exchange-correlation energy functional is not known. With further approximations we have a self consistent equation that can be written as

$$\hat{H}_{ks}\Psi_i(r) = \varepsilon_i\Psi_i(r) \tag{3.13}$$

$$H_{ks}(r) = -\frac{1}{2}\nabla^2 + V_{ks}(r) \tag{3.14}$$

where

$$V_{ks}(r) = V_{ext}(r) + V_{xc}(r) + V_H(r) \tag{3.15}$$

Here $V_{ks}(r)$ is the effective Kohn-Sham potential. From this we have a self consistent set of equations wherein we start with the initial electron density and find the effective Kohn-Sham potential which would be used to solve equation 3.13 to find a new value for the density. As per the Hohenberg-Kohn theorem 2, if the initial and the new density are the same, then the ground state density is found. If not, then we start again with a new initial density and the steps are repeated until convergence is achieved.

3.2 Approximation methods in DFT

Approximation methods make computationally intensive calculations feasible. It is one the important part of studies in DFT calculation. In this section we will look at some of the approximations that are widely used in DFT calculations.

3.2.1 Local Density Approximation

The local density approximation (LDA) is derived from the homogeneous gas theory (HEG). It assumes that the electron density is the same. It determines the exchange correlation energy from the local electron density. This is one of the simplest approach and it works because the errors by under estimation of exchange and over estimation of correlation energy densities cancel out each other and the contribution from the exchange-correlation energy is minimal. It also generates an acceptable estimate of the spherical average.

$$E_{xc}^{LDA} = \int \varepsilon_{xc}(\rho)\rho(r)dr \tag{3.16}$$

The generalized gradient approximation (GGA) is built upon the LDA by expanding the 3.16 in terms of gradient for the density. It provides a good balance between speed and accuracy. It rewrites 3.16 as

$$E_{xc}^{LDA} = \int \varepsilon_{xc}(\rho, \nabla\rho)\rho(r)dr \tag{3.17}$$

3.2.2 Pseudopotential approximation

Bloch's theorem states that the electronic wavefunction can be expressed as a discrete set of plane waves. This consists of a plane wave part and a periodic cell part.

$$\Psi_n(r) = u_n(r)e^{ik.r} \tag{3.18}$$

where $\Psi_n(r)$ is the wavefunction of an election in band n. The periodic part of the wavefunction can be written as

$$u_n(r) = \sum_K c_{i,K}, e(r)^{i(k+K)r} \tag{3.19}$$

Substituting equation 3.19 in 3.18, we get

$$\Psi_n(r) = \sum_K c_(n, K), e^{i(k+K)r} \tag{3.20}$$

Still using this we require a large set of plane wavefunctions for all the electrons and this in turn increases the computation power required to solve them. The pseudopotential method circumvents this problem by utilizing the fact that most of the physical properties of solids are explained by the valence electrons to large extent compared to the core. The core electron in the vicinity of the nucleus and the nuclear potential are replaced with a weaker pseudopotential which acts on a set of pseudo wavefunctions in place of actual valence electron wavefunctions. Outside the core both the potentials are the same. This is exemplified in figure 3.1.

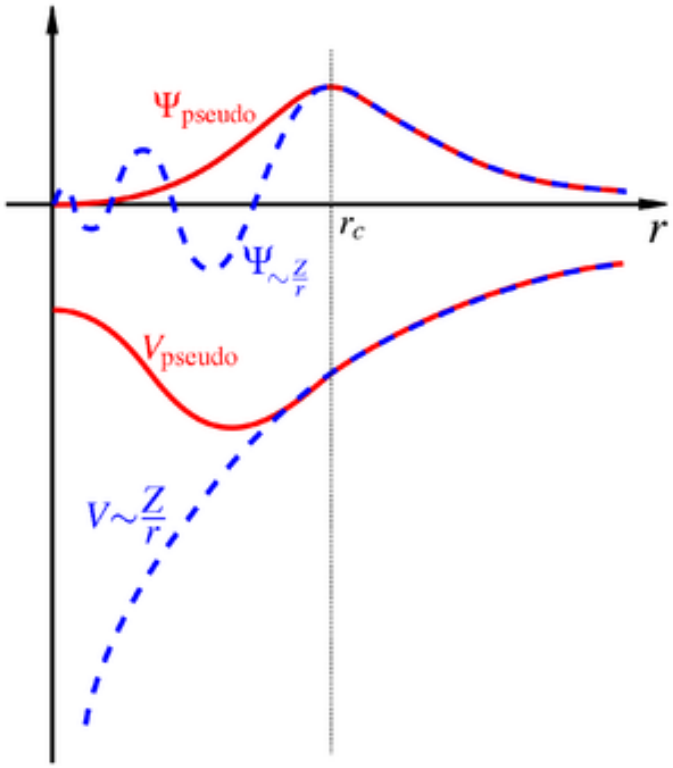

Figure 3.1: Schematic representation of the potentials and their wavefunctions

The radius at which the pseudopotential and the actual potential match is the cutoff radius r_c. For a realistic approach we reduce the cutoff radius but this results in more plane wavefunctions to solve. The ultrasoft pseudopotential is a method building on the pseudopotential violating the norm-conservation. It reduces the number of plane wave basis sets by removing the charge of the orbitals in the core region resulting in a reduction in the cutoff energy.

3.2.3 Augmented plane wave method

Augmented plane wave method approximation (APW) is that the potential is assumed to be spherically symmetric with the centre at the atom's position in the lattice and the potential is a constant in the interstitial region. For a core radius r_0,

$$V(r) = \begin{cases} V(r) & for\, r < r_0 \\ V_0 & for\, r > r_0 \end{cases} \tag{3.21}$$

The radial schrodinger equation for the effective potential is given by

$$\Big[-\frac{\hbar^2}{2m_e} + V_{eff}(r) - E \Big] u = 0 \tag{3.22}$$

where

$$V_{eff}(r) = \Big[\frac{\hbar^2}{2m_e} \frac{l(l+1)}{r^2} + V(r) \Big] \tag{3.23}$$

The wavefunction for the interstitial space is written in terms of plane waves as in 3.20. For the entire crystal, it is a linear combination of the two wavefunctions rewritten as

$$\Psi_k(r) = \begin{cases} \sum_{lm} A_{l,m} U_l(r) Y_{lm}(r) & for\, r < r_0 \\ \sum_K c_{n,K)}, e^{i(k+K)r} & for\, r > r_0 \end{cases} \tag{3.24}$$

The coefficient A_{lm} is determined by matching the two functions at the sphere boundary ($r = r_0$).

3.2.4 Projector augmented wave method

This method was developed as a combination of both the pseudopotential and APW method. It involves linear transformation of the wavefunctions close to the core into auxiliary wavefunctions due to the fact that the wavefunctions near to the core have rapid oscillations and to make it into a smooth wavefunction which is easier to solve. It uses the APW method to describe the wavefunctions near the core and pseudopotential method for the valence electron wavefunctions. The transformation of the actual wavefunction to an auxiliary wavefunction is written as

$$|\Psi_n\rangle = T|\tilde{\Psi}_n\rangle \tag{3.25}$$

This is done only for the wavefunctions close to the core and a cutoff radius is chosen. At the valence region, the partial waves are identical i.e. the auxiliary wavefunction

is the same as the actual wavefunction.The valence electron wavefunction is subtracted from the all electron wavefunction to obtain the auxiliary wavefunctions for the core. [49]

$$|\Psi_n\rangle = |\tilde{\Psi}_n\rangle + \sum_i (|\phi_i\rangle - |\tilde{\phi}_i\rangle)\langle \tilde{p}_i|\tilde{\Psi}\rangle \tag{3.26}$$

3.3 Classical molecular dynamics

Classical molecular dynamics (CMD) simulations treat the interaction between the atoms by ignoring the electrons as in the Born-Oppenheimer approximation and consider only the position of the nuclei. This makes the calculations far less computationally intensive and allows us to simulate for a larger number of atoms and longer time scale as in comparison with DFT. It uses Newton's second law of motion to predict the position of the atoms after each time step. The forces on the atoms are calculated as the vector sum of all the forces resulting from its interaction with all the other atoms from its position at time t and give a new position at time $t + \delta t$. The forces acting on atoms is given by

$$F = m.\frac{\mathrm{d}^2 r}{\mathrm{d}t^2} \tag{3.27}$$

We obtain the position as

$$r = \delta t.\frac{\mathrm{d}r}{\mathrm{d}t} + r(t) \tag{3.28}$$

We discretize the time intervals in 'n' number of sub intervals and we get $\delta t = t_{end}/n$ where n = 0, 1, 2... are the discrete time intervals. We now have $t_{n+1} = t_n + \delta t$ and rewriting equation 3.28 at time t_n

$$v(t_n) = \frac{r(t_{n+1}) - r(t_n)}{\delta t} \tag{3.29}$$

From equation 3.29, the acceleration at t can be given as the change in velocity as

$$a(t_n) = \frac{\frac{r(t_{n+1}) - r(t_n)}{\delta t} - \frac{r(t_n) - r(t_{n-1})}{\delta t}}{\delta t} \tag{3.30}$$

From this we get

$$r(t_{n+1}) = 2r(t_n) - r(t_{n-1}) + a(t_n).\delta t^2 \tag{3.31}$$

The Verlet method uses the position and acceleration at t and position at time t_{n-1} to obtain the position at t_{n+1}. The Taylor expansion of $r(t_{n+1})$ and $r(t_{n-1})$ is given by

$$r(t_{n+1}) = r(t) + \delta t.\frac{\mathrm{d}r(t)}{\mathrm{d}t} + \frac{\delta t^2}{2}.\frac{\mathrm{d}^2 r(t)}{\mathrm{d}t^2} + \mathcal{O}(\delta t^3) \tag{3.32}$$

$$r(t_{n-1}) = r(t) - \delta t.\frac{\mathrm{d}r(t)}{\mathrm{d}t} + \frac{\delta t^2}{2}.\frac{\mathrm{d}^2 r(t)}{\mathrm{d}t^2} - \mathcal{O}(\delta t^3) \tag{3.33}$$

On adding the equations 3.32 and 3.33, we get

$$r(t_{n+1}) = 2r(t) - r(t_{n-1}) + \delta t^2.a(t) + \mathcal{O}(\delta t^4) \tag{3.34}$$

Using this Taylor expansion improves the accuracy of the Verlet integrator method. However here the velocities are not explicitly stated. Using a leap-frog algorithm we can calculate the velocity to find the kinetic energies and temperature at time t by

$$v(t_n) = \frac{r(t_{n+1}) - r(t_{n-1})}{2\delta t} + \mathcal{O}(\delta t^2) \tag{3.35}$$

The equation 3.35 shows that halving the time step can be done but it reduces the accuracy by the same order. The velocity Verlet algorithm explicitly uses the velocity to solve the first timestep problem. This ensures precision as it yield position, velocity and the accelerations at time t.

$$r(t_{n+1}) = r(t) + \delta t.v(t) + \frac{\delta t^2}{2}.a(t) \tag{3.36}$$

$$v(t_{n+1}) = v(t) + \frac{a(t) + a(t + \delta t)}{2}\delta t \tag{3.37}$$

This algorithm works by the following steps:

1. The crystal with a set number of atoms is described at time t.
2. Calculate the forces at time t from the interatomic potential
3. Update the positions at fist time step t_{n+1} from 3.36
4. Evaluate the forces at t_{n+1} from the provided interatomic potential and derive velocity with 3.37
5. Repeat steps with the updated position and velocities as input for the next time step

The positions of the atoms are updated after each time step. The drawback is that if the chosen time step is too large, then we may miss the interaction. Having a small time step prevents this but increases the computation time [50].

3.3.1 Embedded atom method potential

The Embedded atom method (EAM) is a semi-empirical potential for calculating the energy of a many body system. The simplest of interaction potential is the pair-potential which provides the potential as a function of the radial distance between the two atoms and independent of the number of bonds associated with the atom.

$$E_{tot} = \frac{1}{2}\sum_{i,j(i\neq j})V(R_{ij}) \tag{3.38}$$

But in reality, the potential is dependent on the number of bonds associated with the atom. Further developments to this model led to the EAM potential [51, 52]. The potential is described by a pair-potential term $\Phi(r)$ which represents coulomb repulsion between the cores and a cohesive term $F(r)$ representing the embedding energy of the atom in the electron gas cloud which is a function of the electron density ρ. The total energy for N number of atoms is given by

$$E_{tot} = \frac{1}{2}\sum_{i<j}^{N} \Phi_{ij}(r_{ij}) + \sum_{i} F_i\Big(\sum \rho_j(r_{ij})\Big) \tag{3.39}$$

where the density ρ_j is spherically averaged.

4

Cascade modelling

In this chapter the method and tools used for modelling the displacement cascade are described along with the parameters that were chosen for optimization. The work is divided into two parts. First is the optimization of parameters carried out using MD simulations and then the optimized parameters were used to simulate a displacement cascade using AIMD.

4.1 MD simulation condition and parameters

The CMD simulation were carried out using EAM interatomic potentials using Dymoka. It is well suited for simulating systems with large unit cells and metals with valence electrons in the d orbital [53].

4.1.1 Size of super-cell and energy of PKA

The simulations were run in non-cubic BCC iron systems with periodic boundary conditions (PBC) ranging from 1000 atoms to 12000 atoms. The use of non-cubic cells is to avoid the long distance migration of defects due to the applied periodic boundary conditions. Due to the presence of PBC any defect that is moving to the boundary gets back in to the super-cell and by using a non-cubic cell we aim to maximize the self-crossing distance in any direction [54,55]. The energy of the PKA was varied from 200 eV to 1000 eV in steps of 100 eV for all the super-cells. These two parameters are the most important. The cost of computation is high for larger cells. The idea was to find the right energy range for smaller cells which will be used for AIMD.

4.1.2 Direction & position of PKA and damping effects

The cascades were also analyzed for different directions of the PKA due the directional dependence of the threshold energy. The role of the damping effects on the cascades were studied by applying a 0.8Å thermal layer to the boundary to remove the excess energy from the system. A strong damping coefficient would essentially

quench the system and a weak damping effect would not reproduce the effect of an infinite boundary.

The position of the PKA in the cell was also varied. For a PKA in a particular direction if the position is close to the boundary, the cascade evolution is also closer to the boundary. The interaction of the cascade with the boundary and large energy losses to the boundary must be minimized and the resulting creation of defects near to the boundary has to be avoided. This is not a problem in bigger cells but in smaller cells this affects the evolution of the cascade. The evolution of the cascade is in the direction of the PKA away from the center. From the center of the cell, the position of the PKA was brought back along the line of direction of the PKA.

4.1.3 Initial condition for simulation

The initial temperature of the simulation cell was set to 50 K. Once the system is described, positions are assigned to every atom. Upon providing the temperature, velocities are assigned randomly to the atoms as per the Maxwell-Boltzmann distribution. Thermalisation was carried out first maintaining the temperature at 50 K before the creation of the PKA. The evolution of the system is governed by the time step. After analyzing the system, 5 different time steps ranging form 0.05 fs to 2 fs were assigned. Shorter time steps are used for the evolution during the initial stages and longer time steps were used for the later annealing stages. This keeps the simulation times not too long and the shorter time scales at the ballistic phase and thermal spike helps describe the evolution more precisely. The position and size of the cascade, the position of the defects formed and the number of vacancies and interstitials at the end state were studied.

4.2 Ab-initio simulation

Using the input parameters optimized from the first stage in MD simulations, AIMD simulations were carried out in iron using VASP in the Born-Oppenheimer approximation. PAW potentials were used. To speed up the simulation, AIMD simulations were coupled with another CMD tool called LAMMPS which uses a semi-empirical EAM potential to perform simulations [56]. This was done using a code which first predicts the trajectories of the atoms and creates a neighbour list. From this list the code uses two potentials to treat the atoms. It uses a soft PAW potential for iron which treats 3d and 4s as the valence states with a total of 8 electrons and a hard potential which treats 3p as the valence state with a total of 14 electrons. The code utilizes the hard potential if the atoms are closer than a cut-off radius and treats other atoms with the softer potential. A maximum of four iterations of this method was carried out. Since the simulations were run in massively parallel multi-core systems, for both MD and AIMD simulations, parallelization optimization was carried out to ensure optimum utilization of resources.

5

Results and discussions

In this chapter the results of this thesis are discussed. The results from the optimization simulations are analyzed and presented. The first focus is on the influence of cell size and energy of the PKA. It is good to start with this as it is the most important factor. Upon finalizing the energy of the PKA and the cell size, simulations were run to understand the effect of introducing damping on the cell boundaries. By introducing damping effects on the cell boundaries we will be able to perform higher energy simulations in a relatively smaller cell. The effect of this was analyzed by simulating with different energies for PKA in small and large cells. For the final parameter, simulations were run for different positions of PKA and the location of the cascade in the cell was studied.

5.1 Influence of cell size and energy of PKA

Simulations were carried out in non-cubic cells of size 7x8x9 up to 17x18x19 for energies 200 to 1000 eV in steps of 100 eV. The number of defects formed at convergence in each case were studied for different directions including high symmetry directions like $\langle 110 \rangle$ and low symmetry directions like $\langle 135 \rangle$. The plot 5.1 shows the effect of PKA energy on the number of vacancies formed in different cell sizes. From the plot 5.1 we can see that at higher energies there is a lot of variation in the number of vacancies formed and in small cells fewer vacancies means that energy is lost to the boundaries. For energies up to 500 eV, we can see that a minimum cell size of approximately 2600 atoms provides a good result. For energies above 500 eV, even at cell sizes up to 11000 atoms had some variations. This clearly shows that the cell size is one of the important deciding factors for choosing the energy of the PKA.

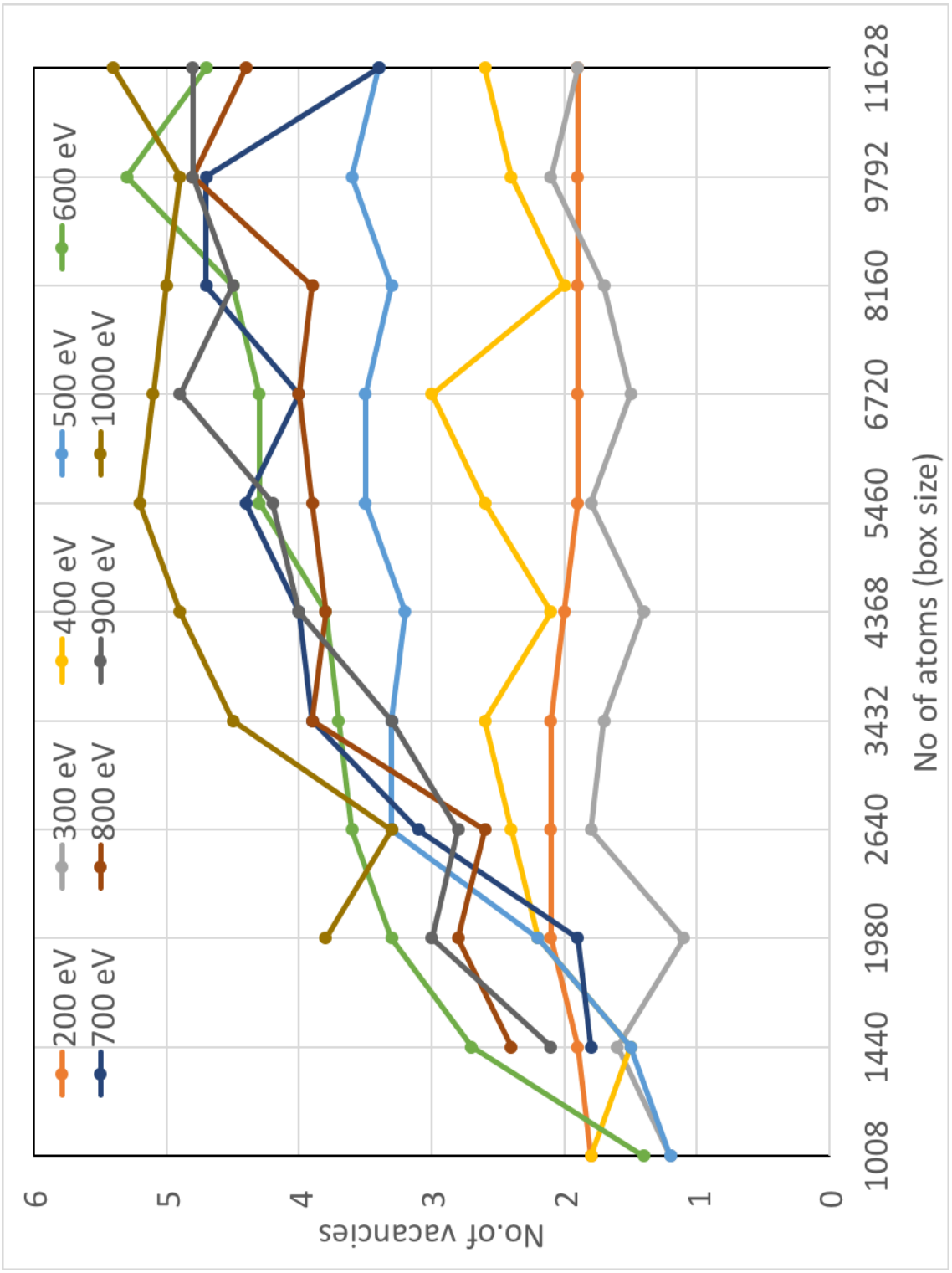

Figure 5.1: Number of vacancies vs cell size for direction ⟨135⟩

The plot 5.2 shows the standard error in the results. For higher energies the error is visibly higher. Each case was run for ten times to obtain some statistics. For the higher energy cases more runs would be required to have a lower error percentage.

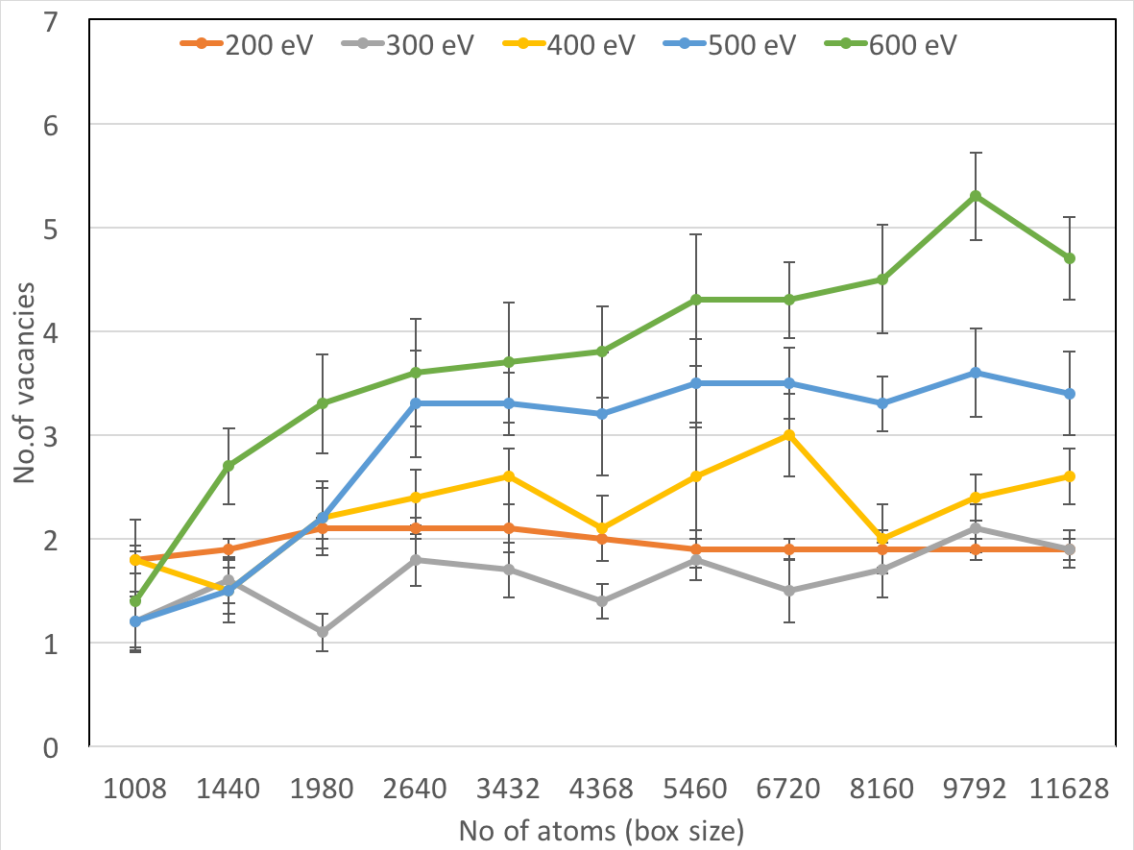

Figure 5.2: Standard error in simulations

The below plot 5.3 shows the number of vacancies formed for a 300 eV PKA in different directions. We can see that the low symmetry directions like ⟨135⟩ and ⟨123⟩ had lower number of vacancies formed. The directional dependence of the threshold displacement energy (TDE) results in lower number of vacancies formed in the ⟨135⟩ and ⟨123⟩ as they have lower TDE compared to the high symmetry directions like ⟨110⟩ or ⟨100⟩. In iron the highest threshold energies occur roughly around the ⟨123⟩ direction [57] which is as expected in the results.

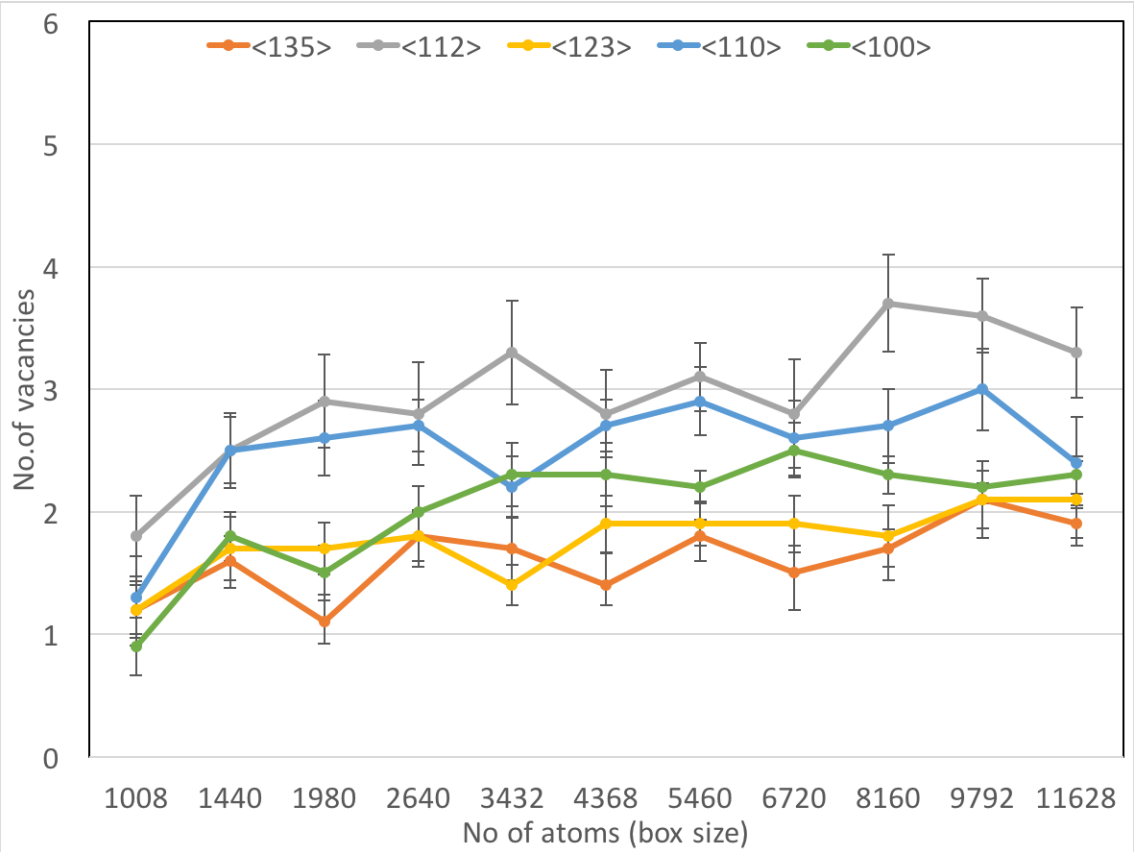

Figure 5.3: Comparison of defect formation in different directions (300eV)

From the results, it was concluded that to perform simulations with an energy of 400 eV for the PKA a minimum cell size of 2000 atoms is required and for 500 eV a minimum of 2500 atoms are required for the ⟨135⟩ PKA direction. The forthcoming section provides further insight about performing simulations for higher energies of PKA.

5.2 Damping effects on the boundary

Before the introduction of the PKA, the cell was thermalised at 50K. Simulations were run using different damping coefficients at 50K for regions of 0.8Å around the border for two different cell sizes of 1980 atoms and 5460 atoms. The results comparing both the cells are presented in the plot 5.4. The presented results are for a 300 eV PKA in ⟨135⟩ direction. The dotted lines labelled as 200L, 300L and so on represent the larger cell and the solid lines labelled as 200S, 300S and so on represent the smaller cell. We can see that at lower energies the damping applied on the borders did not have a significant effect. From an optimum damping coefficient of $1e^{-10}$, we can see that the number of vacancies formed for energies 200 and 300 eV are similar in both cells. For energies 500 and 600 eV we can see the difference in the number of vacancies between the large and small cells.

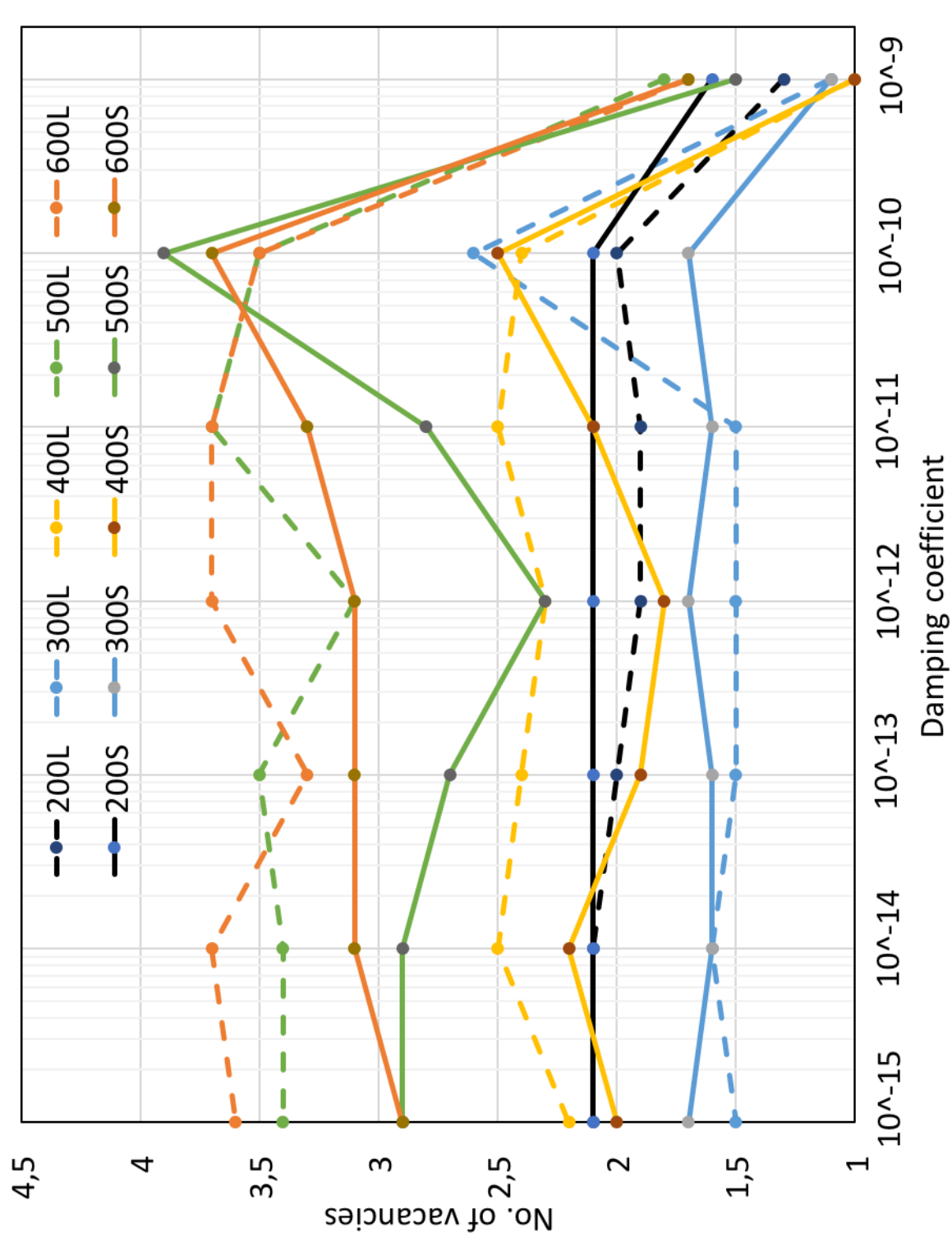

Figure 5.4: Effect of damping on large and small cells (300ev in $\langle 135 \rangle$)

The damping applied was more efficient in removing the energy from the small cell suggesting that we will be able to do higher energy simulations in a small cell with the right damping coefficient for a given case. By having an optimum damping coefficient for reasonably higher energies we will be able to perform simulation in smaller cells by having a virtually infinite lattice thereby reducing the computation required.

5.3 Effect of position of the PKA

The size of the cascade in a simulation is dependent on the energy of the PKA. Interaction of the cascade with the boundary must be avoided to prevent energy losses to the boundary. While introducing a PKA in a particular direction we chose an atom close to the center and we shoot it away from the center. We performed simulations with different positions of the PKA as shown in the figure 5.5. The idea is to bring back the PKA along the direction we will be introducing it and away from the centre.

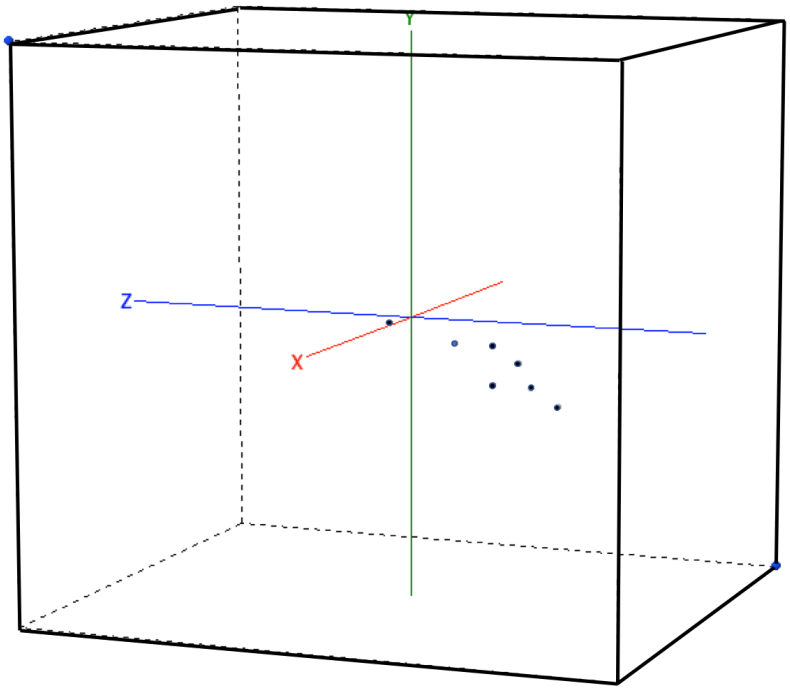

Figure 5.5: Different positions for the PKA

In a large cell as the one shown in the plot 5.6, the solid line represents the simulations with the PKA's position in the center and the dotted lines are the simulations for which the positions were altered with A being the furthest away from the center and G being the closest. By bringing back the PKA along a line perpendicular to the $\langle 135 \rangle$ plane away from the center, the cascade it generates is also brought away from the boundary and closer to the center.

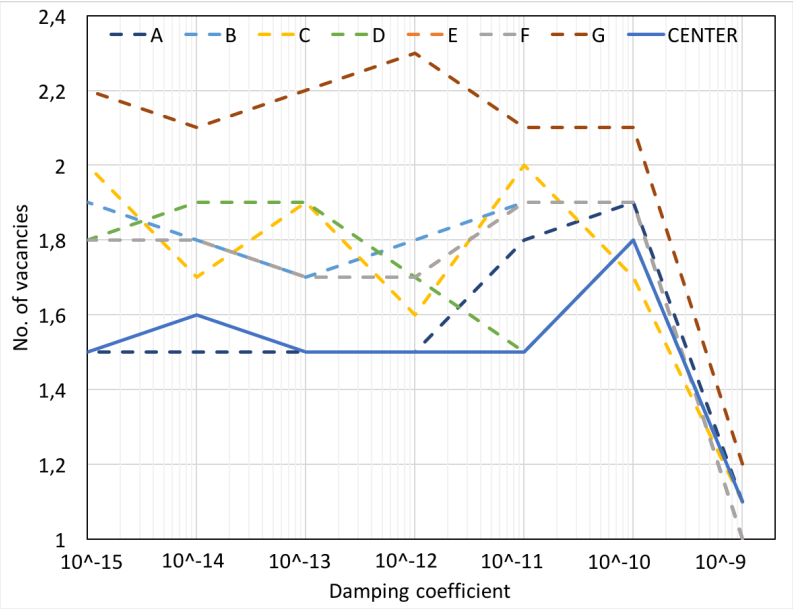

Figure 5.6: Effect of PKA positions in a large cell (300ev in ⟨135⟩ for 5460 atoms)

From the plot, we can see that the number of vacancies resulting from the PKA's new positions were higher than from its position in the center. This can be due to the loss of energy during the evolution of the cascade when the position of the PKA is closer to the boundary in the direction we are introducing it. However, in a smaller cell (see figure 5.7), the variation in the position of PKA also affected the number of vacancies formed. But the effect was much lower compared to a larger cell. This also can be attributed to the damping that was applied to the border in these cases and since it is a smaller cell, some of the energy from the cascade was lost to the boundary.

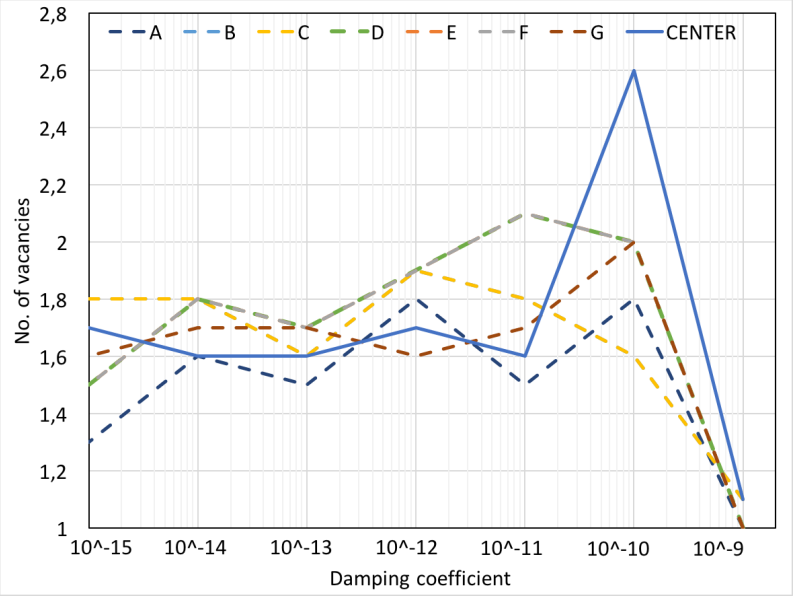

Figure 5.7: Effect of PKA positions in a large cell (300ev in ⟨135⟩ for 1980 atoms)

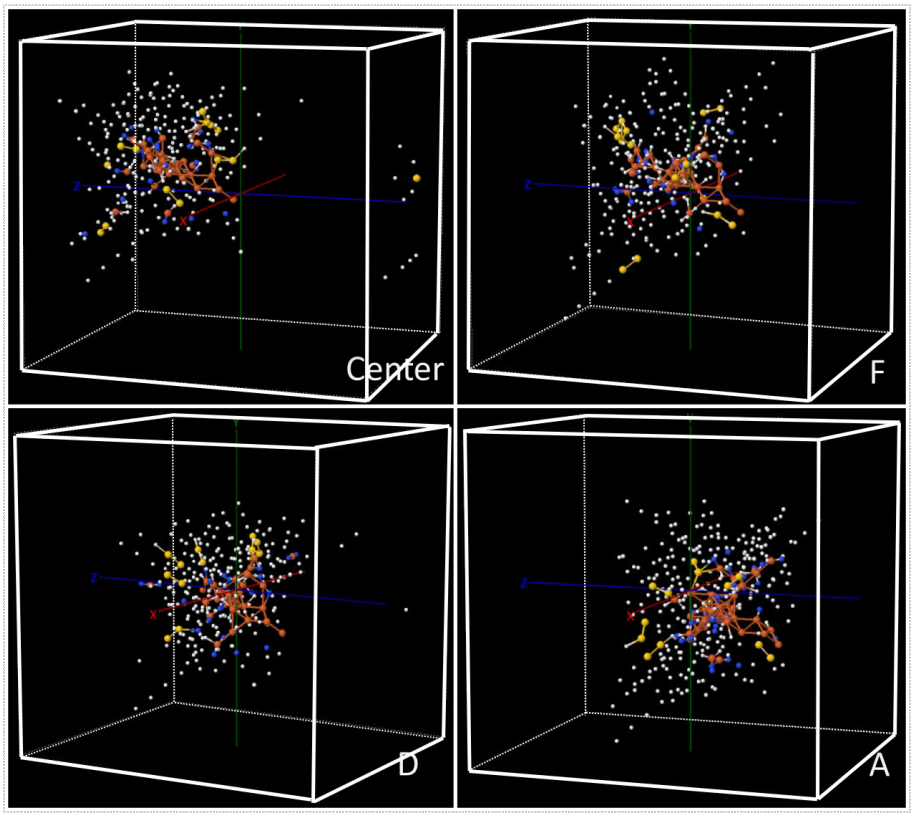

Figure 5.8: Effect of PKA positions in a large cell (500ev in ⟨135⟩ for 5460 atoms)

The figure 5.8 shows the size of the cascade and its location inside the cell for different positions of the PKA. With the position A being the furthest we can clearly see the position of the cascade brought back away from the boundary. From the figures 5.6 and 5.7 we can observe that this method is more effective in larger cells.

6

Conclusions

Understanding the effect of radiation in the structural materials of a nuclear reactor is paramount for us to design reactor that can operate for a long period in a safe manner. The reactor pressure vessel is one the most important safety barrier in a nuclear power plant. It shields us from all kinds of radiations emitted from the reactor core. This leads to degradation of the material over time in many different ways. It can affect the hardness, ductility, brittleness, etc., of the material which can lead to a failure which can be catastrophic. Molecular dynamics and DFT are some of the tools that can be used to study the effects of radiation on these materials.

The different methods and approximations that are used to model the radiation effects were studied. Using molecular dynamics, the different input parameters that are required to perform simulations were analyzed and optimized. The goal was to perform various simulations varying all the input parameters considered for this work and study the cascade evolution and defects formed due to neutron irradiation. The results were thoroughly processed and the data required to be visualized were plotted.

By performing simulations for varying cell sizes with low to high energy PKAs, we were able to decide on the maximum energy of the PKA that we can simulate for a given cell size. For a PKA of 500 eV energy we require a minimum cell size of approximately 2500 atoms. Using this parameter further simulations were performed for different positions of the PKA and damping effects on the border of the cell.

The different dampings that were applied to the small and large boxes provided a better understanding about the effects of having a damping. At lower energies of PKA, the damping does not affect the number of defects formed in both larger and smaller cells. For higher energies of PKA, the damping provided was able to remove the energy near the boundaries effectively in smaller cells compared to the larger cells. This is because the cascade evolving inside the cell is much closer to the boundary in smaller cells. Using this we understood that it is possible to perform simulations with higher energy PKAs in relatively smaller cells by providing damping conditions in the border.

Similarly, varying the position of the PKA did not have much effect in smaller cells whereas at higher energies in a larger cell we were able to effectively bring the cascade away from the boundary. Overall, by using the optimal cell size for a given energy and by using an effective damping coefficient for the borders and position

for the PKA, we will be able to perform simulations with high energy PKA without having to increase the cell size by a significant amount.

6.1 Future Work

From the results obtained from this work, we have started AIMD simulations in VASP. For the first stage we have started running simulations in a box of 1980 atoms and 300 eV of energy for the PKA. These AIMD simulations take much longer time compared to the MD simulations that were carried out in the first stage of this work.

The results from the first stage of MD simulations performed in this work has been positive and this gives the foundation to take this work to the next level by performing simulations increasing the energy to the order of 1,000 to 2,000 eV in supercells of 10,000 to 20,000 atoms to see the effects of damping and different positions of the PKA.

Bibliography

[1] KSU AB, "Huvudprocessen, kraftindustrins grundutbildningspaket," vol. E-087, 2005.

[2] B.M. Gordon, "Corrosion and corrosion control in light water reactors," *JOM.*, vol. 65, p. 1043, 2013.

[3] J.D. Lawson, "Some criteria for a power producing thermonuclear reactor," *Proceedings of the Physical Society. Section B*, vol. 70, no. 1, p. 6, 1957.

[4] T. Fülöp and I. Pusztai, "Fusion energy: Lecture notes." Chalmers University of Technology, 2015.

[5] CEA France, "Magnetic fusion: The main principles." `http://www-fusion-magnetique.cea.fr/gb/fusion/principes/principes01.htm`. Online; accessed 2017/10/25.

[6] M.A. Prelas, "Direct conversion of nuclear energy to electricity," *Int. Sci. J. Altern. Energy Ecology*, vol. 2,9, 2007.

[7] N. Rostoker, M. Binderbauer, and H. Monkhorst, "Colliding beam fusion reactor," *Science*, vol. 278, no. 5342, pp. 1419–1422, 1997.

[8] P. Norajitra, L. Boccaccini, *et al.*, "Development of a helium-cooled divertor: Material choice and technological studies," *J. Nucl. Mater.*, vol. 367-370, no. Part B, pp. 1416 – 1421, 2007.

[9] P. Norajitra, S. I. Abdel-Khalik, *et al.*, "Divertor conceptual designs for a fusion power plant," *Fusion Eng. Des.*, vol. 83, no. 7, pp. 893 – 902, 2008.

[10] F. Granberg, K. Nordlund, *et al.*, "Mechanism of radiation damage reduction in equiatomic multicomponent single phase alloys," *Phys. Rev. Lett.*, vol. 116, p. 135504, 2016.

[11] S. V. M. Rieth, S.L. Dudarev *et al.*, "Recent progress in research on tungsten materials for nuclear fusion applications in europe," *J. Nucl. Mater.*, vol. 432, no. 1, pp. 482 – 500, 2013.

[12] A. Hasegawa, M. Fukuda, *et al.*, "Neutron irradiation effects on the microstructural development of tungsten and tungsten alloys," *J. Nucl. Mater.*, vol. 471, no. Supplement C, pp. 175 – 183, 2016.

[13] A. E. Sand, M. J. Aliaga, M. J. Caturla, and K. Nordlund, "Surface effects and statistical laws of defects in primary radiation damage: Tungsten vs. iron," *EPL*, vol. 115, no. 3, p. 36001, 2016.

[14] C. Domain, "Ab initio modelling of defect properties with substitutional and interstitials elements in steels and zr alloys," *J. Nucl. Mater.*, vol. 351, no. 1, pp. 1 – 19, 2006.

[15] M. Thuvander, "Irradiation effects on rpv steel: Lecture notes." Chalmers University of Technology, 2016.

[16] H. Ullmaier and W. Schilling, "Radiation damage in metallic reactor materials," *Physics of Modern Materials*, vol. 1, IAEA, Vienna, 1980.

[17] G. Kinchin and R. Pease, "The displacement of atoms in solids by radiation," *Reports on Progress in Physics*, vol. 18, pp. 1–51, 1955.

[18] W. Snyder and J. Neufeld, "Disordering of solids by neutron radiation," *Phys. Rev.*, vol. 97, no. 6, p. 1636, 1955.

[19] J. Lindhard, V. Nielsen, and M. Scharff, "Approximation method in classical scattering by screened coulomb fields," *Mat. Fys. Medd. Dan. Vid. Selsk.*, vol. 36, no. 10, 1968.

[20] M. Norgett, M. Robinson, and I. Torrens, "A proposed method of calculating displacement dose rates," *Nucl.Eng.Des*, vol. 33, pp. 50–54, 1975.

[21] G. S. Was, *Fundamental of Radiation Materials Science.* Springer Berlin Heidelberg, 2 ed., 2017.

[22] D. Bacon, A. Calder, and F. Gao, "Defect production due to displacement cascades in metals as revealed by computer simulation," *J. Nucl. Mater.*, vol. 251, no. Supplement C, pp. 1 – 12, 1997.

[23] C. Becquart, A. Souidi, C. Domain, M. Hou, L. Malerba, and R. Stoller, "Effect of displacement cascade structure and defect mobility on the growth of point defect clusters under irradiation," *J. Nucl. Mater.*, vol. 351, no. 1, pp. 39 – 46, 2006.

[24] D. J. Bacon, A. F. Calder, and F. Gao, "Computer simulation of displacement cascade effects in metals," *Radiation Effects and Defects in Solids*, vol. 141, no. 1-4, pp. 283–310, 1997.

[25] A. Sand, K. Nordlund, and S. Dudarev, "Radiation damage production in massive cascades initiated by fusion neutrons in tungsten," *J. Nucl. Mater.*, vol. 455, no. 1, pp. 207 – 211, 2014.

[26] A. Calder, D. Bacon, A. Barashev, and Y. Osetsky, "Effect of mass of the primary knock-on atom on displacement cascade debris in α-iron," *Philos. Mag. Lett.*, vol. 88, no. 1, pp. 43–53, 2008.

[27] A. Calder, D. Bacon, A. Barashev, and Y. Osetsky, "On the origin of large interstitial clusters in displacement cascades," *Philos. Mag.*, vol. 90, no. 7-8, pp. 863–884, 2010.

[28] T. Diaz de la Rubia, M. Caturla, E. Alonso, M. Fluss, and J. Perlado, "Self-decay-induced damage production and micro-structure evolution in fcc metals: An atomic-scale computer simulation approach," *J. Comput-Aided Mater.*, vol. 5, pp. 243–264, May 1998.

[29] C. Barouh, T. Schuler, C.-C. Fu, and T. Jourdan, "Predicting vacancy-mediated diffusion of interstitial solutes in α-fe," *Phys. Rev. B*, vol. 92, p. 104102, Sep 2015.

[30] D. Terentyev, L. Malerba, R. Chakarova, K. Nordlund, P. Olsson, M. Rieth, and J. Wallenius, "Displacement cascades in Fe–Cr: A molecular dynamics study," *J. Nucl. Mater.*, vol. 349, no. 1, pp. 119 – 132, 2006.

[31] A. F. Calder, D. J. Bacon, A. V. Barashev, and Y. N. Osetsky, "Computer simulation of cascade damage in α-iron with carbon in solution," *J. Nucl. Mater.*, vol. 382, no. 2, pp. 91 – 95, 2008. Microstructural Processes in Irradiated Materials.

[32] R. Ngayam-Happy, C. Becquart, C. Domain, and L. Malerba, "Formation and evolution of mnni clusters in neutron irradiated dilute fe alloys modelled by a first principle-based akmc method," *J. Nucl. Mater.*, vol. 426, no. 1, pp. 198 – 207, 2012.

[33] L. Messina, M. Chiapetto, P. Olsson, C. S. Becquart, and L. Malerba, "An object kinetic monte carlo model for the microstructure evolution of neutron-irradiated reactor pressure vessel steels," *physica status solidi (a)*, vol. 213, no. 11, pp. 2974–2980, 2016.

[34] G. S. Was, J. P. Wharry, B. Frisbie, B. D. Wirth, D. Morgan, J. D. Tucker, and T. R. Allen, "Assessment of radiation-induced segregation mechanisms in austenitic and ferritic–martensitic alloys," *J. Nucl. Mater.*, vol. 411, no. 1, pp. 41 – 50, 2011.

[35] S. Bruemmer, E. Simonen, P. Scott, P. Andresen, G. Was, and J. Nelson, "Radiation-induced material changes and susceptibility to intergranular failure of light-water-reactor core internals," *J. Nucl. Mater.*, vol. 274, no. 3, pp. 299 – 314, 1999.

[36] C. M. Barr, G. A. Vetterick, *et al.*, "Anisotropic radiation-induced segregation in 316l austenitic stainless steel with grain boundary character," *Acta Materialia*, vol. 67, no. Supplement C, pp. 145 – 155, 2014.

[37] S. Song, R. Faulkner, P. Flewitt, P. Marmy, and M. Victoria, "Grain boundary phosphorus and molybdenum segregation under irradiation and thermal conditions in a 2.25cr1mo steel," *Mater. Sci. Eng. A*, vol. 286, no. 2, pp. 230 – 235, 2000.

[38] R. Faulkner, S. Song, P. Flewitt, M. Victoria, and P. Marmy, "Grain boundary segregation under neutron irradiation in dilute alloys," *J. Nucl. Mater.*, vol. 255, no. 2, pp. 189 – 209, 1998.

[39] D. Meade, R. Faulkner, and D. Ellis, "Radiation-induced grain boundary segregation of phosphorus in asme sa533b ferritic pressure vessel steel," *ASTM STP 1366*, vol. 1366, pp. 383–398, 2000.

[40] T. Takeuchi, Y. Kakubo, Y. Matsukawa, *et al.*, "Effects of neutron irradiation on microstructures and hardness of stainless steel weld-overlay cladding of nuclear reactor pressure vessels," *J. Nucl. Mater.*, vol. 449, no. 1, pp. 273 – 276, 2014.

[41] T. Takeuchi, Y. Kakubo, Y. Matsukawa, *et al.*, "Effect of neutron irradiation on the microstructure of the stainless steel electroslag weld overlay cladding of nuclear reactor pressure vessels," *J. Nucl. Mater.*, vol. 443, no. 1, pp. 266 – 273, 2013.

[42] S. Kotrechko, V. Dubinko, N. Stetsenko, D. Terentyev, X. He, and M. Sorokin, "Temperature dependence of irradiation hardening due to dislocation loops and precipitates in rpv steels and model alloys," *J. Nucl. Mater.*, vol. 464, no. Supplement C, pp. 6 – 15, 2015.

[43] G. S. Was, *Fundamental of Radiation Materials Science.* Springer Berlin Heidelberg, 2 ed., 2017.

[44] M. Thuvander, "Lecture on ss hardening, swelling and creep." Chalmers University of Technology, 2016.

[45] T. Williams and D. Arkell, "Void-swelling in 20% cold-worked fv548 austenitic stainless steel irradiated with 22 mev c2+ ions or 46.5 mev ni6+ ions," *J. Nucl. Mater.*, vol. 80, no. 1, pp. 79 – 87, 1979.

[46] Y. Chen, "Irradiation effects of ht-9 martensitic steel," *NET.*, vol. 45, no. 3, pp. 311 – 322, 2013.

[47] P. Hohenberg and W. Kohn, "Inhomogeneous electron gas," *Phys. Rev.*, vol. 136, pp. B864–B871, Nov 1964.

[48] W. Kohn and L. J. Sham, "Self-consistent equations including exchange and correlation effects," *Phys. Rev.*, vol. 140, pp. A1133–A1138, Nov 1965.

[49] P. E. Blöchl, "Projector augmented-wave method," *Phys. Rev. B*, vol. 50, pp. 17953–17979, Dec 1994.

[50] M. Griebel, S. Knapek, and G. Zumbusch, *Numerical Simulation in Molecular Dynamics: Numerics, Algorithms, Parallelization, Applications.* Springer Publishing Company, Incorporated, 1st ed., 2010.

[51] M. S. Daw and M. I. Baskes, "Embedded-atom method: Derivation and application to impurities, surfaces, and other defects in metals," *Phys. Rev. B*, vol. 29, pp. 6443–6453, Jun 1984.

[52] S. M. Foiles, M. I. Baskes, and M. S. Daw, "Embedded-atom-method functions for the fcc metals cu, ag, au, ni, pd, pt, and their alloys," *Phys. Rev. B*, vol. 33, pp. 7983–7991, Jun 1986.

[53] M. S. Daw, S. M. Foiles, and M. I. Baskes, "The embedded-atom method: a review of theory and applications," *Mater. Sci. Eng., R*, vol. 9, no. 7, pp. 251 – 310, 1993.

[54] P. Olsson, C. S. Becquart, and C. Domain, "Ab initio threshold displacement energies in iron," *Mater. Res. Lett.*, vol. 4, no. 4, pp. 219–225, 2016.

[55] L. Malerba, C. S. Becquart, and C. Domain, "Object kinetic monte carlo study of sink strengths," *J. Nuc. Mater.*, vol. 360, no. 2, pp. 159 – 169, 2007.

[56] D. Karlsson and A. Salvolainen Rasmussen, "Optimization of vasp simulations relating to radiation damage in materials," 2017.

[57] K. Nordlund, J. Wallenius, and L. Malerba, "Molecular dynamics simulations of threshold displacement energies in fe," *Nucl. Instrum. Methods Phys. Res., Sect. B*, vol. 246, no. 2, pp. 322 – 332, 2006.